Title

Water level changes in Lake Erie drive 21st century CO2 and CH4 fluxes from a coastal temperate wetland

Authors

Morin, Timothy H

Riley, William J

Grant, Robert F

et al.

Publication Date

2022-05-01

DOI

10.1016/j.scitotenv.2022.153087

Water level changes in Lake Erie drive 21st century CO_2 and CH_4 fluxes from a coastal temperate wetland

Timothy H. Morin [1], William J. Riley [2], Robert F. Grant [3], Zelalem Mekonnen [2], Kay C. Stefanik [4], A. Camilo Rey Sanchez [5], Molly A. Mulhare [1], Jorge Villa [6], Kelly Wrighton [7], Gil Bohrer [8]

1 – Department of Environmental Resources Engineering, State University of New York College of Environmental Sciences and Forestry

2 – Climate and Ecosystem Sciences Division; Lawrence Berkeley National Laboratory

3 – Department of Renewable Resources, University of Alberta

4 – College of Agriculture and Life Sciences, Iowa State University

5 – Department of Marine, Earth and Atmospheric Sciences. North Carolina State University.

6– School of Geosciences, University of Louisiana at Lafayette

7 – Soil and Crop Sciences, Colorado State University

8– Department of Civil, Environmental and Geodetic Engineering, The Ohio State University

Abstract

Wetland water depth influences microbial and plant communities, which can alter the above- and below-ground carbon cycling of a wetland. Wetland water depths are likely to change due to shifting precipitation patterns, which will affect projections of greenhouse gas emissions; however, these effects are rarely incorporated into wetland greenhouse gas models. Seeking to address this gap, we used a mechanistic model, *ecosys*, to simulate a range of water depth scenarios in a temperate wetland, and analyzed simulated predictions of carbon dioxide (CO_2) and methane (CH_4) fluxes over the 21st century. We tested our model using eddy covariance measurements of CO_2 and CH_4 fluxes collected at the Old Woman Creek National Estuarine Research Reserve (OWC) during 2015 and 2016. OWC is a lacustrine, estuarine, freshwater, mineral-soil marsh. An empirical model found that the wetland water depth is highly dependent on the water depth of the nearby Lake Erie. Future wetland surface water depths were modeled based on projection of Lake Erie's water depth using four separate NOAA projections, resulting in four wetland water-depth scenarios. Two of the four 21st century projections for Lake Erie water depths used in this study indicated that the water depth of the wetland would remain nearly steady; however, the other two indicated decreases in the wetland water depth. In our scenario where the wetland dries out, we project the wetland's climatological warming effect will decrease due to smaller CH_4 fluxes to the atmosphere and larger CO_2 uptake by the wetland. We also found that increased water level can lower emissions by shifting the site towards more open water areas, which have lower CH_4 emissions. We found that decreased water depths would cause more widespread colonization of the wetland by macrophyte vegetation. Using an empirical relationship, we also found that further drying could result in other, non-wetland vegetation to emerge, dramatically altering soil carbon cycling. In three of our four projections, we found that in general the magnitude of CO_2 and CH_4 fluxes steadily increase over the next 100 years in response to higher temperatures. However, in our driest simulations, we projected a different response due to increased oxidation of soil carbon, with CH_4 emissions decreasing substantially from an annual cumulative peak of 224.6 to a minimum of 104.7 gC m^{-2} $year^{-1}$. In that same simulation, net cumulative flux of CO_2 changed from being a sink of 56.5 gC m^{-2} $year^{-1}$ to a source of 369.6 gC m^{-2} $year^{-1}$ over the same period, despite a temperature increase from 13.7°C to 14.2°C. This temperature shift in our other three cases with greater water depths increased the source strength of CH_4 and the sink strength of CO_2.

We conclude that the magnitude of wetland greenhouse-gas fluxes depended on the water depth primarily as it affected the areal percentage of the wetland available for plant colonization, but dramatic decreases in water depths could cause significant reductions in the wetland CH_4 fluxes, while simultaneously altering the wetland vegetation.

1. Introduction

Wetlands occupy a unique niche in the global carbon cycle: they can serve as important CO_2 sinks through carbon fixation and important CO_2 sources via microbial respiration, they are one of the largest terrestrial reservoirs of organic carbon, and they are major sources of methane (CH_4), a powerful greenhouse gas (GHG). Wetland CO_2 and CH_4 vertical fluxes result from a complex set of interdependent carbon, nutrient, water, and energy flux dynamics, making current forecasting efforts rather uncertain (Melton et al., 2013; Poulter et al., 2017; Saunois et al., 2019). Ecological variables, such as wetland surface-water depths, affect many underlying carbon cycling processes, often in opposing ways.

Wetland water depths affect a myriad of important biogeochemical and plant processes that, in turn, affect GHG fluxes. Primarily, water depth affects wetland GHG fluxes through effects on plants, effects on microbes, and changes to turbulent transport of compounds.

Water depth's effects on plants are significant for wetland carbon cycling since plants are typically a major source of organic carbon for most wetlands (Nowak et al., 2015). Both the type and abundance of wetland plants are strongly affected by the depth of standing water (Colmer, 2003; Strand, 2002). Many wetland plants have adaptations for anoxic (oxygen limited) conditions in the root zone (e.g., via larger aerenchyma, Armstrong, 1980; Laan et al., 1989), thus water depths can stimulate or suppress plant growth (Armstrong, 1980; Colmer, 2003; Justin and Armstrong, 1987; Sorrell et al., 2000; Strand, 2002). Changing the vegetation structure also directly affects CH_4 flux by affecting gas transport rates. Aerenchyma provide a substantial pathway of CH_4 transport to the atmosphere (Garnet et al., 2005; Jeffrey et al., 2019; Kao-Kniffin et al., 2010; Sutton-Grier and Megonigal, 2011; Villa et al., 2020). Beyond these effects, water depth changes can also drive shifts in abundance and diversity of wetland plants over a longer time span, affecting CH_4 fluxes (Lenssen et al., 1999; Seabloom et al., 2001; Keddy and Ellis, 1985; Seabloom et al., 1998).

Microbial communities are similarly affected by water depth, which can drive changes in ecosystem carbon cycling (Elberling et al., 2011). Water depth alters electron acceptor availability in the soil, particularly oxygen, by creating a barrier for vertical transport of oxygen into the soil (Elberling et al., 2011). Changes in vegetation community structures also have major effects on rates of oxygen transport to the soil as they can move large quantities of oxygen through their lacunar root system (Colmer, 2003).

As water depths are likely to change in many wetlands, it is important to have modeling tools that can estimate the likely effects that this change will have, but few models explicitly account for each of these processes, leaving our predictions in this regard speculative and poorly constrained. Lacustrine temperate wetlands, particularly in the Great Lakes region, have highly uncertain forecasts for water depths, which,

combined with the relative complexity of the underlying carbon processes and their interactions, have resulted in relatively poor capability to predict these wetlands' carbon budget.

Here we sought to address this gap by using the mechanistic, process-based model *ecosys* (Grant et al., 1997), in which the biogeochemical processes controlling methanogenesis and methanotrophy are explicitly represented, to develop an understanding of how water depth affects CH_4 fluxes from a temperate freshwater estuarine wetland in northern Ohio, and applied the model to predict 21st century fluxes. Although *ecosys* has been used for a wide range of purposes, the work here builds upon its use for wetland CH_4 fluxes.

We evaluated the model performance by comparing its predictions to eddy covariance CO_2 and CH_4 flux data gathered under known water depths at the wetland from 2015 to 2016 at Old Woman Creek (OWC). Using observations from the site, we developed empirical models to predict the water depth and plant community structure of the wetland from regional meteorological conditions and water depths at Lake Erie, which is partially hydrologically linked to the wetland. We then used *ecosys* with water depths predicted from the empirical relationships between lake and wetland water depths, and climatologic projections of Lake Erie water depths to investigate wetland plant-community dynamics, CO_2 and CH_4 fluxes, and carbon storage over the 21st century.

2. Methods

2.1 Site description

Old Woman Creek (OWC) National Estuarine Research Reserve (NERR) (Figure 1), located at Lake Erie's southern shore (41.378° N latitude, 277.489° E longitude), is operated jointly between the National Oceanic and Atmospheric Administration (NOAA) and the Ohio Department of Natural Resources (ODNR). The site's land cover can be roughly classified into four types: open water, mud flats, patches of emergent cattail vegetation (*Typha spp.*), and patches of floating-leaved vegetation (co-dominated by *Nelumbo* spp. and *Nymphaea* spp.). During 2015 and 2016 the dominant plant species of the wetland was *Typha* spp, which occupied 78% of the vegetated area in 2015.

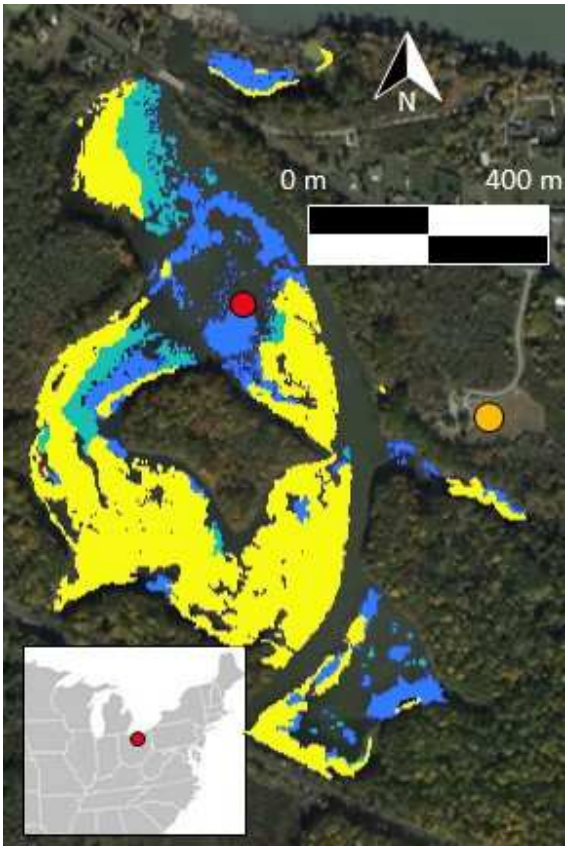

Figure 1. The Old Woman Creek National Estuarine Research Reserve, which served as the model training site for this analysis. Colors on the map are vegetation cover in 2015, when data for the site were first collected. Each color represents a different species of wetland vegetation, with yellow representing stalk bearing emergent macrophytes (mostly Typha spp. *and some Phragmites Australis), blue representing Nelumbo spp., and green representing other floating-leaved macrophyte vegetation (e.g. Nymphaea* spp.). *Area of open water was digitized for analysis but is not shown here for clarity. Red dot on map indicates the eddy-covariance tower location. Orange dot indicates location of a meteorological station.*

OWC is a natural freshwater, temperate, mineral-soil, estuarine marsh, fed by the tributary Old Woman Creek. Through much of the year, a sand barrier separates Lake Erie from Old Woman Creek. The barrier breaches and reforms on a roughly semi-annual basis. When the barrier breaches, OWC and Lake Erie are hydrologically linked. The breaches often happen when the water depth in the wetland and the water depth in Lake Erie are disparate, which drives water movement through the sand barrier and thereby bank erosion. The result is a rapid equilibration of Old Woman Creek with Lake Erie's water depth, and a rapid shift in the wetland water depth. The barrier reforms over time (typically within 3-5 weeks after the barrier break, but some times faster) as waves deposit sand and sediment from the lake at the river mouth.

2.2 Meteorological, hydrological, and eddy covariance measurements

The OWC eddy-covariance (EC) tower has been in operation since May 2015 and is registered with the Ameriflux network (Site-ID: US-OWC (Bohrer et al., 2015)) (Figure 1). The site is equipped with open-path IRGAs for CO_2/H_2O and CH_4 (LI-7500 and LI-7700, LI-COR Biosciences, Lincoln, NE) and an ultrasonic anemometer (CSAT3, Campbell Sci.), installed roughly 3 m above the ground (which could be flooded, roughness length and footprint calculations include a half hourly update of the surface elevation based on the water depth). The tower also measures air temperature and humidity (HMP155, Vaisala, Helsinki, Finland), incoming and outgoing radiation (NR01, HuskeFlux, Delft, The Netherlands) and has a network of soil temperature probes (107L, Campbell Scientific, Logan, UT) to provide the soil temperature gradients at three locations in the wetland. Chamber measurements were conducted monthly in multiple locations of different patch types throughout the wetland. The chamber measurement data and the patch type maps for the site at different years are available through ESS-DiVE (Bohrer et al., 2019). The flux calculation approach for this tower has been previously described by Rey-Sanchez et al (2018) and is based on the formulation used at another wetland site by Morin et al (2014a, b). In brief, we applied a 3-D wind rotation to force the average vertical and cross wind components for each half hour to be zero (Lee et al., 2004). We allowed for slight time lags between our two data series (vertical wind perturbations and solute concentration), performing a constrained time-lag technique based on the maximal covariance approach (Detto et al., 2011). All fast data time series were despiked by looking for extreme outliers (i.e. greater than 6 standard deviations away from a local temporal neighborhood of points). We applied standard WPL and frequency response corrections to fluxes (Webb et al., 1980; Massman, 2000). We applied an empirical seasonal threshold u* value that filtered data out when flux data were significantly correlated to u* (Reichstein et al., 2005), and set a minimum value for u* at 0.2 m/s. We assumed the same u* threshold was sufficient for CO_2 and CH_4 and based our filter on the CO_2 fluxes for both. Finally, we utilized a footprint model to quantify the relative contribution of each land-cover type to the site-level flux observation during a particular half hour. We used a multi-patch expansion of the 2-D footprint model developed by Detto et al (2006), which is an expansion of the 1-D model developed by (2000).

A nearby meteorological station and several water quality and level gauges are run at by the OWC NERR staff (NOAA, ODNR). These provided additional hydrological and water quality data. Particularly, we used the wetland water depth and dissolved oxygen concentration (DO). Data are publicly available through NOAA's NERR website at http://cdmo.baruch.sc.edu/). We obtained 12 years (2005-2016) of data and performed gap-filling using a bi-linear periodic function as described in Morin et al (2014a). We obtained Lake Erie water depth data from 2000-2016 using NOAA data gathered at the

Marblehead station (publicly available through NOAA Tides and Currents, 'Marblehead, OH' station, Station Code: 9063079, https://tidesandcurrents.noaa.gov/).

2.3 Model Description

We parameterized and evaluated the model *ecosys* (Grant et al., 2017b, a; Grant, 1997) for the OWC site. *Ecosys* is an hourly time-step model that mechanistically tracks the thermodynamics, hydrology, and nutrient cycling of an ecosystem in up to 3 dimensions using linked grid-cells and discretized soil and canopy layers. *Ecosys* is widely used (approximately 100 peer-reviewed studies), and performs well in model inter-comparison studies (Amthor et al., 2001; Dietze et al., 2011; Hanson et al., 2004; Matheny et al., 2014). It has been used in a wide range of terrestrial ecosystems (Grant, 2013; Grant et al., 1999; Grant and Roulet, 2002), including wetlands (Dimitrov et al., 2014b, a; Grant et al., 2012; Mezbahuddin et al., 2014). *Ecosys* is built around a coupled thermodynamic and hydrologic scheme with a simultaneous solution for soil temperature and soil moisture. The model uses energy budget closure to iterate for latent heat fluxes consistent with canopy water potential and overall system energy and water budgets. Sub-hourly sub-surface hydrology is simulated using a discretized mixed case of Richard's equation for unsaturated flow, Darcy and Green-Ampt equations for saturated flow with infiltration and ponding, and a Poiseuille equation for macropore flow.

Ecosys features detailed vegetation and biogeochemistry representations that are relevant to this study. For vegetation, *ecosys* uses interacting multi-layer plant-canopy and root system profiles that represent plant growth, competition, and succession. Each plant functional type (PFT) is described through a suite of PFT properties including photosynthetic pathway (C3, C4), annual or perennial, evergreen or deciduous, vascular or nonvascular, and N_2 fixing or non-N_2 fixing.

Its biogeochemistry module is a multi-phase model that explicitly resolves biomasses of diverse microbial functional types (MFT) subject to stoichiometric and bioenergetic constraints. The biogeochemistry of *ecosys* is particularly appropriate for modeling CH_4 since it explicitly represents: (1) oxidation-reduction reactions driven by microbial communities composed of relevant microbial guilds with transient population sizes; (2) thermodynamic, substrate, and inhibition constraints on microbial respiration and growth by which these reactions are driven; and (3) aqueous and gaseous phase processes and transport in soil and roots. CH_4 generation and consumption are described in Grant and Roulet (2002) and in Grant et al. (2012). Biological CH_4 processes are included in *ecosys* to simulate the interrelated activities of MFTs for anaerobic fermenters, which produce hydrogen and acetate, acetotrophic methanogens, and hydrogenotrophic methanogens. The basis of the microbial simulation is a stoichiometric mass conservation and the energetics of the oxidation-reduction transformations mediated by each MFT. *Ecosys* couples soil biogeochemistry and vegetation dynamics driven by competition (e.g.,

plant roots and microbes using a limited soil O_2 and nutrient supplies) and symbiosis (e.g., mychorrhizal fungi) for soil nutrients. Aerenchyma in modeled vegetation also serves as a transmission pathway for oxygen into the soil and for greenhouse gases to escape from the soil, providing an important biogeochemical interaction between the two modules. In this study, all model parameters remained the same as those in studies cited earlier (e.g. (Grant et al., 2012; Grant and Roulet, 2002; Chang et al., 2020, 2019)).

2.3.1 Soil parameters

Ecosys requires a detailed description of the soil physical and chemical properties as domain descriptors and initial conditions for the model. Appendices A1-3 tabulates all soil parameters and initial values used in this study and details the sources. Here we itemize some of the most critical sources for the model soil inputs. Bulk density values were obtained from Bernal and Mitsch (2008). These observations extended 60 cm into the soil, and we assumed them constant for deeper layers. Initial concentration profiles for SO_4, Fe, NO_3, and pH were measured from soil core samples using a modified mooring-system soil corer. Fe (II) was measured by mixing 1 g of soil with added to 5 mL 0.5N HCl in a 15 mL disposable centrifuge tube and vortexed. We allowed samples to sit overnight for dissociation. 20µl of the soil/HCL mix was then placed into a 15 mL disposable centrifuge tube containing 4.8 mL of dionized water. One Hach FerroVer Iron Reagent for 5 mL sample packet was added to each tube and the tube was vortexed for 2 minutes, and then run on a spectrophotometer at 510 nm for absorbance. Ion chromatography was used to determine [NO_3] and [SO_4] in the geochemistry soil cores at various depths. 5 g of soil was added to 5 mL of deionized water in a 15 mL falcon tube and vortexed to create a soil slurry. An pH/mV meter (AB150 , Accumet, Westford, MA, USA) was used to measure pH of the soil slurry. The soil slurry was then passed through a 0.2 um filter. The filtered liquid was stored in 2 ml microcentrifuge tubes at -20°C until analysis on an Ion Chromatography System (ICS-2100, Dionex, Sunnyvale, CA) with an AS18 column.

Sand, silt, and clay percentages, hydraulic conductivity, cation and anion exchange capacities, organic nitrogen, organic phosphorus, aluminum, calcium, magnesium, sodium, and potassium concentrations were determined at multiple depths by extracted cores, which were segregated into 5 cm depths down to 30 cm. The Colorado State University Soil, Water, and Plant Testing Lab analyzed the cored soil samples.

Volumetric water content at field capacity, and at wilting point were estimated using the Soil-Plant-Atmosphere-Water (SPAW) model (Rawls et al., 1982; Saxton and Rawls, 2006). We used the SPAW soil water characteristics tool for this purpose and provided it with the soil texture (i.e. sand, silt, clay) and the organic content of the soil. All other *ecosys* inputs were taken from previously validated *ecosys* runs

of a generalized 0.25×0.25 km^2 grid cell representing northern Ohio within a full-scale North America run (Mekonnen et al., 2016).

2.3.2 Model forcing for historical period: meteorological conditions and water depth

We used air temperature, wind speed, relative humidity, precipitation, and incoming short wave radiation data from the OWC meteorological station to create the model's weather forcing files for 1956 – 2019 based on data from 2006-2016. *Ecosys* uses an external water table with a prescribed depth to drive discharge and recharge across lateral boundaries within which internal water tables are modeled (Mezbahuddin et al., 2014). The depth of this external water table can be allowed to change during model runs. We chose to directly drive *ecosys* with the measured ecosystem surface water depth as a prescribed hourly variable because the hydrologic behavior of Old Woman Creek depends on the breaching and reformation of a sand barrier at the point where the wetland meets Lake Erie. We accomplished this by setting the external water table to a negative (i.e. aboveground) value equal to the measured standing water depth at each hourly time step. We obtained the hourly water depth data from gauges at OWC, adjusted to correspond to the water depth around the eddy covariance tower's footprint area. We adjusted the model inputs that controlled the lateral equilibration of surface water with the external water table to regulate the grid-cell water depth within each time step. We also disabled sediment flow simulated with the surface-water flow. There is uncertainty associated with this approach, since some sediment mass is likely lost to Lake Erie when the lake and the wetland are connected. However, we believe this loss to have relatively small implications for the wetland mass budgets of greenhouse gasses at annual timescales, compared to other potential sources of error. We used data from Lake Erie water depths to drive an empirical model for the wetland water depth for 21st century projections (see section 2.3.5.2 21st century water depth forcing).

We spun-up the model using 10 years (2005-2014) of meteorological data, looped five times to simulate a period of 50 years (from 1956 to 2005), initializing all PFTs in 1956. We used additional 11 years of data as part of the explicit simulation period (2006-2016), and actual data for 2015 and 2016 instead of looped data values. We determined that 40 years was an adequate spin-up period by confirming that at the end of the spin-up period the divergence of decadal carbon uptake from the previous decade was less than 1%.

2.3.3 Patch-level simulations of OWC

In most wetland models, the wetland is considered a single tile supporting a single set of forcing and land-cover characteristics. However, in wetlands there are distinct differences between areas within the wetland that are covered with different land cover types, such as open water and macrophyte vegetation. These patches have very different carbon and methane fluxes (Rey-Sanchez et al., 2018; Villa et al., 2020, 2019), as well as different characteristic biogeochemical variables. To handle these different patches, we

set a simulation featuring two interacting grid cells that shared common meteorological forcing for the purpose of calculating the total site-level fluxes. The only difference between the grid cells was that we initialized *Typha* and a sub-aquatic plant species as the active PFTs in 1956 in the vegetated grid cell and only initialized the sub-aquatic species in the open water grid cell. Although *ecosys* can represent several interacting PFTs, we lumped the observed macrophyte PFTs into the single *Typha* PFT for computational efficiency, effectively treating the *Typha* PFT as a stand-in for all possible vegetated cover types at the OWC site. This assumed lack of higher PFT resolution is probably associated with some uncertainty. There are datasets for flux rates and conductivity of methane transport through different vegetation PFTs throughout OWC (see Villa et al (2020) and Bohrer et al (2019). However, due to the relative lack of representation of PFTs other than *Typha* and open water in the EC-tower observation footprint, including other PFTs would have resulted in a largely unconstrained contribution to the model. Though the PFTs in each grid cell were prescribed, PFT productivity within each cell was allowed to vary as predicted by the conditions in the cell, resulting in cases where the conditions in the patch were not suitable for the prescribed vegetation and thus times where the patch was far less productive.

The full model domain encompassed 10×10 m^2, and the two grid cells shared a 10 m long border, which ran North to South through the model domain. We gave each grid cell a width proportional to its relative contribution to the total area during all times where we could quantify the area of each cover type (i.e., the vegetated and open water grid cells were 6.6×10 m^2 and 3.4×10 m^2, respectively). Both grid cells shared the same surface air temperature, humidity, wind, and incoming radiation forcing. They also shared the same water depth fluctuations, though the water depth in the open water patch was set 0.3 m deeper than in the vegetated patch.

We compared *ecosys* flux outputs to those observed by the EC-tower by scaling the two grid cells' (one vegetated, one open water) fluxes to the site level proportional to their relative representation in the EC-tower's observation footprint area at each half hour.We combined the resulting fluxes of each grid cell off-line for predictions of the site-level fluxes using an area-weighted average, from the relative area covered by each patch type. Two types of site-level predictions were made: one based on the whole site area, the other on the relative area of each patch type within the half-hourly flux tower observation footprint area. Whole-site fluxes were used to discuss the model results and predictions. Footprint area predictions were used to compare model and EC-flux observations.

2.3.4 Characteristic of Plant Functional Types in the vegetated patch

During the period where EC data were available for model evaluation, i.e., growing seasons of 2015-2016, the dominant PFT in the site was *Typha* spp. (Figure 1). Floating leaved plants (such as the ones most common in OWC: *Nelumbo lutea* and *Nymphaea odorata*) formed the second most common plant PFT, but the lotus patches had sparse vegetation and we assumed that their ecosystem function was

similar to *Typha* spp. as both are stalk bearing emergent macrophytes with similar gas transport structures. Parameters for *Typha* spp. were taken from a PFT for sedges as developed for *ecosys* (Mekonnen et al., 2016). We adjusted the leaf inclination angles and the leaf length to width ratio to match physical observations in the OWC site. We based the root porosity on similar observed porosities for other wetland plants (i.e. sedges in the range of 33-50% of the root tissue). We then made slight adjustments to the root porosity of *Typha* as a fitting parameter, aiming to match CO_2 and CH_4 flux observations from the eddy covariance tower, when the open water and vegetated grid cells were aggregated to the tower footprint level. We tuned this variable (within reasonable ranges compared to observed values) since the modeled fluxes were quite sensitive to the root porosity and a broad range of values exists for this plant property in the literature. We also initialized sub-aquatic vegetation in both grid-cells. We used a plant functional type for lichens for this purpose. Although we expect that lichens have considerably different functional behavior than sub-aquatic vegetation would in reality, our primary aim with the sub-aquatic vegetation here was to provide a marginal carbon input to both grid cells, preventing the open water cell from depleting its carbon reserves causing a decline of the MFT biomasses that would be modelled in the prolonged absence of any C inputs. The overall contribution of the sub-aquatic vegetation to the site level integrated CO_2 fluxes is small, and so we anticipate only a small amount of error associated with this assumption. Lateral redistribution of dissolved organic carbon (DOC) from the vegetated cell also served as a carbon supply to the open water cell.

2.3.5 21st century model projections

2.3.5.1 21st century climate forcing

We used climatological and hydrological forecasts to create simulated 21st century scenarios based on the Intergovernmental Panel on Climate Change (IPCC) RCP8.5 synthesis (Pachauri et al., 2014), which appears to be a likely climatological forecast scenario. We also selected this climate change scenario because it most closely matched foundational assumptions involved with the Lake Erie water depth models that we used for predictions (Lofgren et al., 2011). We used RCP8.5 air temperature, relative humidity, and precipitation projections (Eyring et al., 2016; Meehl et al., 2000) downscaled to the OWC site location to derive seasonal changes for every year from 2000 to 2100, and then imposed the anomalies on the observed 2005-2014 meteorological record (with CO_2 increasing from 399 ppm in 2014 to 936 ppm in 2100 and temperature increasing 6.44 °C by 2100). In this way, we maintain observed high-frequency climate variability and projected long-term climate changes. Lake Erie water-level projections were taken from Lofgren et al. (2011) using four scenarios based on different projections that differed with regard to the assumptions around the potential evapotranspiration (i.e. whether using temperature or energy budget closure as a proxy for potential evapotranspiration) and the climate model used to drive the Great Lakes model resulting in four water depth cases: (1) Canadian Global Circulation

Model using an Alternative Energy Adjustment Formulation (referred to here as Lake Erie Water depth model 1 or LEWL1 for short) that attempts to close the modeled energy budget. (2) CGCM using the Delta method, which uses temperature as a proxy for potential evapotranspiration (LEWL2). (3) Geophysical Fluid Dynamics Laboratory model using the Alternative Energy Adjustment Formulation (LEWL3). (4) GFDL using the Delta method (LEWL4).

2.3.5.2 21st century water depth forcing

In reality, many factors drive the OWC water depth: precipitation, transpiration, river inflow, shifting wetland bathymetry, the depth of Lake Erie, and the status of the sand barrier between the wetland and the lake. Daily data of sand barrier presence had been collected by a site manager using visual inspection since 1981. Barrier formation and breach are stochastic events that govern much of the water depth dynamics at OWC and add a major hurdle to accurate prediction of water depths at OWC, and similar estuarine wetlands. We used observed water-level data from the NOAA-NERR-operated Lower Estuary (Station code OWCOLWQ), Darrow Road (OWCDRWQ), and the State Route 6 (code OWCWMWQ) gauges at OWC. Water-level data was subject to quality control by removing all data point that were flagged by NOAA diagnostic, and all points that exceeded 6 standard deviations above the mean of a 100-observations moving average. Data were reported at 15-minute intervals, which we averaged to hourly data for use with *ecosys*. The Lower Estuary was used as the 'true' water depth since it is the closest to the eddy covariance station, but data from the other two were used to gap-fill the Lower Estuary data where it was missing and any of the other two were available. This was done by fitting a linear regression between each pair of gauge stations, then using the resulting equation to predict the water depth at the Lower Estuary based on data from any of the other two stations.

We fitted a stepwise multiple linear regression model to predict the observed water depth as a function of water temperature, hourly precipitation rate, relative humidity, PAR, and Lake Erie water depth. We also included a variable that tracked the amount of precipitation accumulation since the barrier last re-formed as a positive value, and the amount of rain that had occurred since it last breached as a negative value. We did the same for the cumulative time before or after a breach. Finally, we added the interaction term between Lake Erie level and the time since barrier breach or formation. For future projections, we assumed breaches would occur at the same times of year as had been previously observed. The resulting empirical model was then used to simulate the wetland water depths during future climate scenarios.

2.3.5.3 Empirical vegetation-cover model

Temperate-wetland plant communities typically senesce in autumn and regrow from rhizomes and seedbanks in spring, causing the plant-community structure to shift in both distribution and abundance each year. We estimated the spatial distribution of wetland plant-communities during future scenarios using an empirical model, which we fitted to the wetland covered by macrophyte vegetation in each year

as a function of water and soil conditions in the spring, when the vegetation established for the year. We treated this as the area in the wetland that macrophytes could grow in each year, and we used *ecosys* to predict the vigor and abundance of the plants within that area. Therefore, from year to year, the percent of the wetland surface area that was available to macrophyes shifted in response to water depth and the density of plants within that area shifted in response to the full range of plant stressors incorporated in *ecosys*. These stressors included those for oxygen, temperature, water, nitrogen, and phosphorus.

We observed the vegetation structure at the wetland in 2015 using a manual ground-based survey. We manually classified site level aerial imagery from the National Agriculture Imagery Program (NAIP, https://www.fsa.usda.gov/programs-and-services/aerial-photography/imagery-programs/naip-imagery/) using ArcGIS to delineate vegetation from open water in 2011, 2013, 2015, and 2017. We created a false-color composite using the near-infrared band combined with the true red band to do the supervised classification, using 2015 as the training basis.

To parameterize the vegetation cover model, we fitted a stepwise linear regression model relating the percentage of the site surface area covered by plants (from classified NAIP images, 2011-2017) to DO, soil temperature, and wetland water depth between April and June. These variables were available from the nearby NOAA-NERR water quality stations that include the water depth gauges. We used the result of the vegetation cover model to do off-line scaling of the vegetated and open-water grid cells into a single, more accurate, whole-site prediction of fluxes.

2.3.5.4 Successional shifts of the wetland vegetation

In low water depth scenarios, surrounding woody vegetation may be able to colonize the wetland. To account for this possibility, whenever the predicted water depth dropped below the surface for more than 30 days, *ecosys* seeded the wetland with 0.001 virtual plants per m^2 of broadleaf seedlings. *Ecosys* automatically reseeds a plant that fails during a model run due to adverse conditions. We first confirmed that, with no standing water, *ecosys* projected the plant functional type of broadleaf trees would be able to grow at the site across the 21st century. For three of the four 21st-century water depth scenarios the standing water depth remained high enough to prevent broadleaf trees plant functional types from growing in the wetland since it remained flooded throughout the simulation. However, in the lowest water depth simulation, broadleaf trees did establish in year 2044.

2.4 Model evaluation

All model evaluations were performed in Matlab (Mathworks, Natick, MA). We evaluated the model against the eddy covariance measurements by determining the model R^2, slope, bias, and root mean squared error. In all cases, we evaluated the model by weighting each of the two grid cells within the effective hourly eddy covariance measurement footprint, which we aggregated from the two measured half hourly footprints. In addition to these standard model evaluation metrics, we performed a Morley

wavelet analysis (Hatala et al., 2012) to evaluate the dependence of observed and modeled CH_4 fluxes on water depth at different periodicities and times. For this analysis, which requires continuous data, we used the gap-filled data from the 2016 growing season and disregarded 2015 due to the frequent gap-filling needed in that year.

In all cases, we use 'flux' as a net vertical exchange with the atmosphere, adopting the atmospheric science sign convention of a positive flux being towards the atmosphere and a negative flux indicating uptake by the ecosystem.

3. Results and Discussion

Empirical water depth model: Figure 2 shows the results of the empirical stepwise linear regression model that predicts the water depth of OWC based on a collection of predictor variables. Overall, our empirical model predicted water depth observations well ($r^2 = 0.48$, bias <0.001 cm, root mean squared error of 17.32 cm, Figure 2a). In recent years (2017-2020), OWC levels were exceptionally high. The reason for these recently high-water depths is not clear, and our stepwise linear model underestimated OWC levels in these extreme years. During the calibration and validation period (2015-2016), *ecosys* simulations used the observed water depths (with rare gaps filled using the model); therefore, the model under-prediction of extreme water did not affect the boundary conditions of *ecosys*.

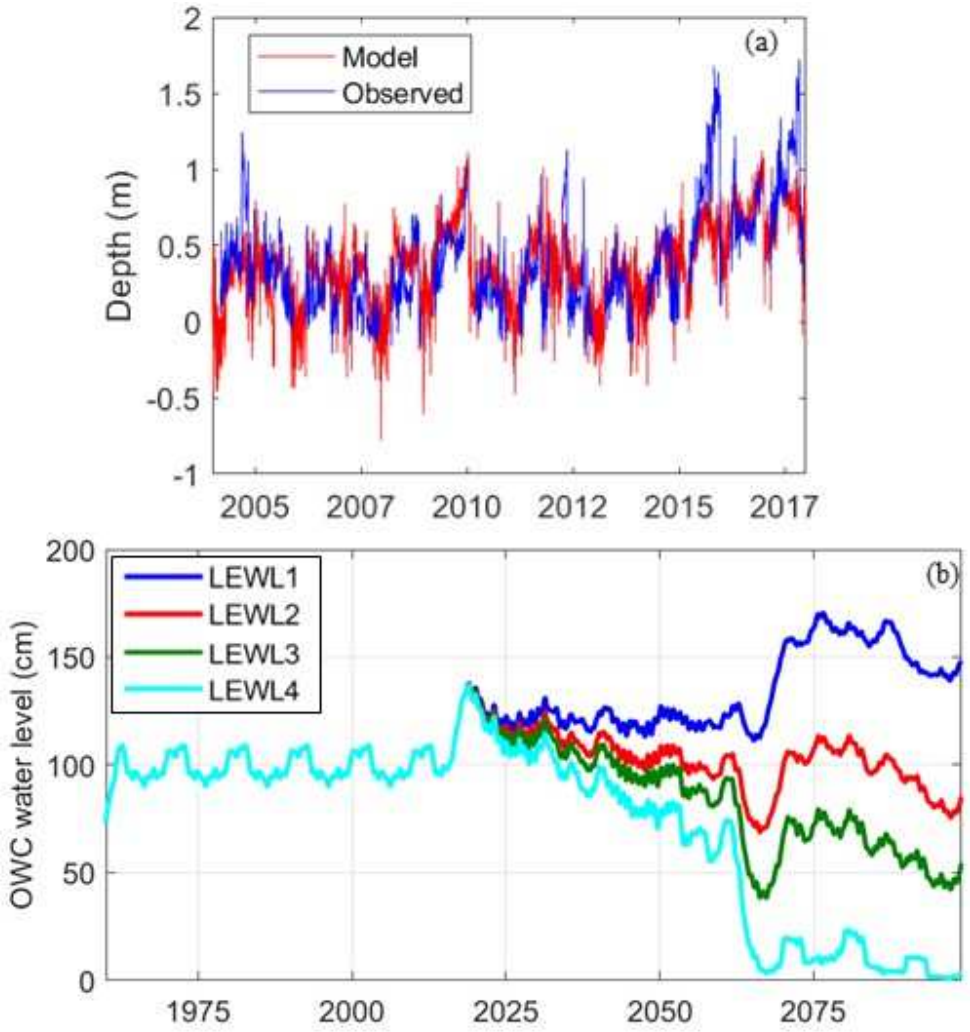

Figure 2. (a) Empirical water depth model for Old Woman Creek (red), generated from the stepwise linear model given in Table A3.1, and gap-filled observations (blue). Gap-filled points were not included in the model's goodness of fit evaluation. Since summer 2015 water depths were anomalously high, which led to underestimation of water depths in that period, especially in the summers. (b) OWC water depth scenarios used for the model simulations. Only scenario LEWL4 had water depths reduced sufficiently to allow broadleaf tree establishment. Water depths have been smoothed here for clarity.

The four scenarios of Lake Eric water depth (LEWL) resulted in an ensemble of possible 21st century water depth scenarios at Old Woman Creek that we used to drive our projections (Figure 2b). Three of these scenarios have the wetland remaining flooded to varying degrees: scenario LEWL1 has an increase in water depth of approximately half a meter, LEWL2 has a nearly stationary water depth, and LEWL3 has a decrease in water depth of ~0.5 m. The fourth water-level scenario (LEWL4) projected that Lake Erie, and correspondingly, OWC water depths will decrease enough to begin drying out the wetland soil. The drawdown to a state of 'no standing water' affected the site as it led *ecosys* to allow establishment of the broadleaf tree PFT, which colonized the formerly flooded area of the wetland.

3.3 Wetland vegetation cover model

The empirical vegetation cover model was used to predict the percentage of the wetland area covered by macrophyte vegetation during each growing season, assuming the reminder of the wetland area is open water. The final empirical model used only water depth as an explanatory variable for observed vegetation cover, with $r^2 = 0.49$. Table A3.By combining the water depth model with the vegetation cover model, we created a model that simulates the hydro-ecological conditions in OWC. While the water depth prediction was used directly as forcing for the model, vegetation areal coverage (which is calculated from water depth) was used to scale the contributions of each of the virtually linked *ecosys* simulated grid cells (open water grid cell, and vegetated grid cell) into the combined site-level fluxes.

Our estimate of the percentage of the OWC wetland occupied by macrophyte vegetation and open water resulted in a decrease in area available for plant colonization as water depth increases. A drawdown in water depth resulted in a larger area available for plant colonization (Figure 3). This relationship caused macrophyte vegetation to increase in LEWL3 and LEWL4. Conversely, LEWL1 saw a reduction in wetland surface area available for macrophyte colonization (bottoming out at nearly 40% of the wetland available for colonization) as its water depths increased with time.

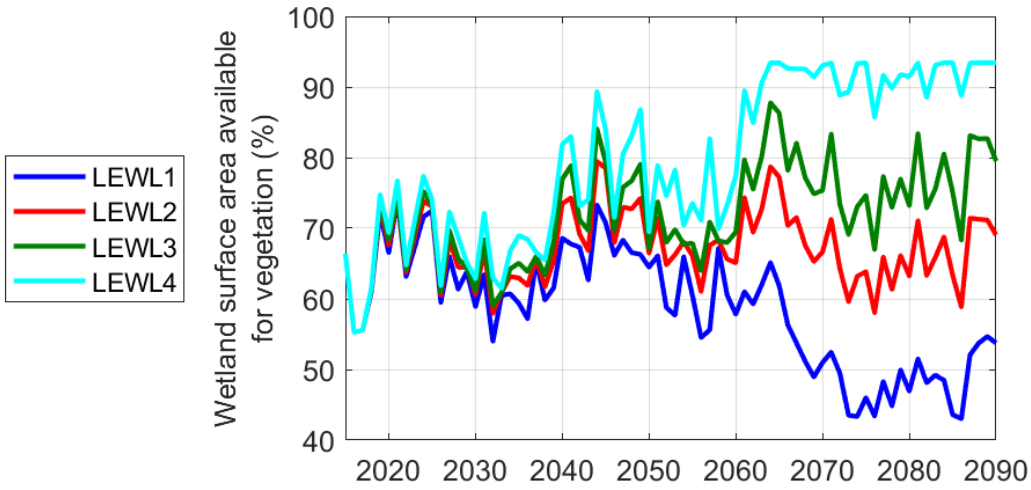

Figure 3. Percentage of the wetland available to be colonized by macrophyte vegetation under the four water depth scenarios. Predicted seed establishment at the wetland is inversely related to the water depth, consistent with increased oxygen availability during the early growing season.

3.4 Evaluating *ecosys* CH_4 and CO_2 vertical flux estimates

Eddy covariance measurements of CH_4 and CO_2 fluxes in OWC during 2015-2016 have been previously reported (Angle et al., 2017; Bohrer et al., 2015; Rey-Sanchez et al., 2018; Villa et al., 2019). OWC is characterized by high magnitude and high variability of CH_4 fluxes (Figure 4). Half hourly CH_4

fluxes ranged from -0.24 µmol m^{-2} s^{-1} to 3.39 µmol m^{-2} s^{-1} in 2015 and 0.03 µmol m^{-2} s^{-1} to 2.11 µmol m^{-2} s^{-1} in 2016. Within the growing season, fluxes displayed an intra-seasonal pattern, peaking in August each year, roughly concomitant with vegetation leaf area at the site.

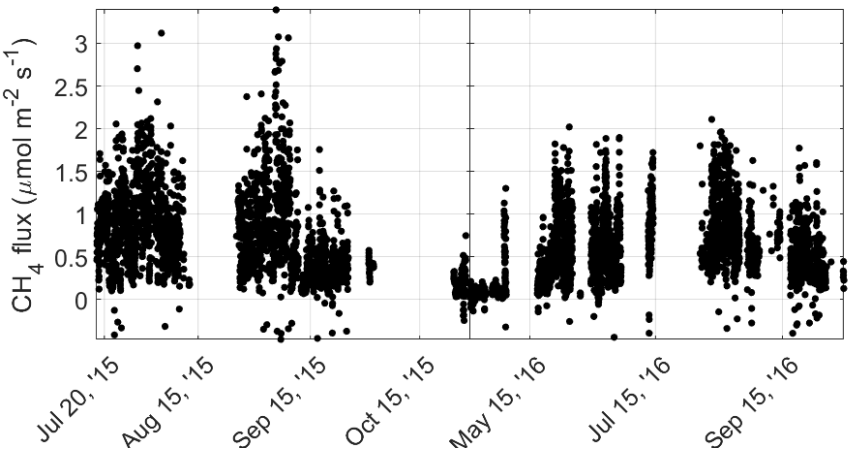

Figure 4. Observed CH_4 fluxes at OWC for 2015 and 2016 growing seasons. Flux rates were high compared to other contemporary mid-latitude, freshwater, marsh sites (Knox et al., 2019).

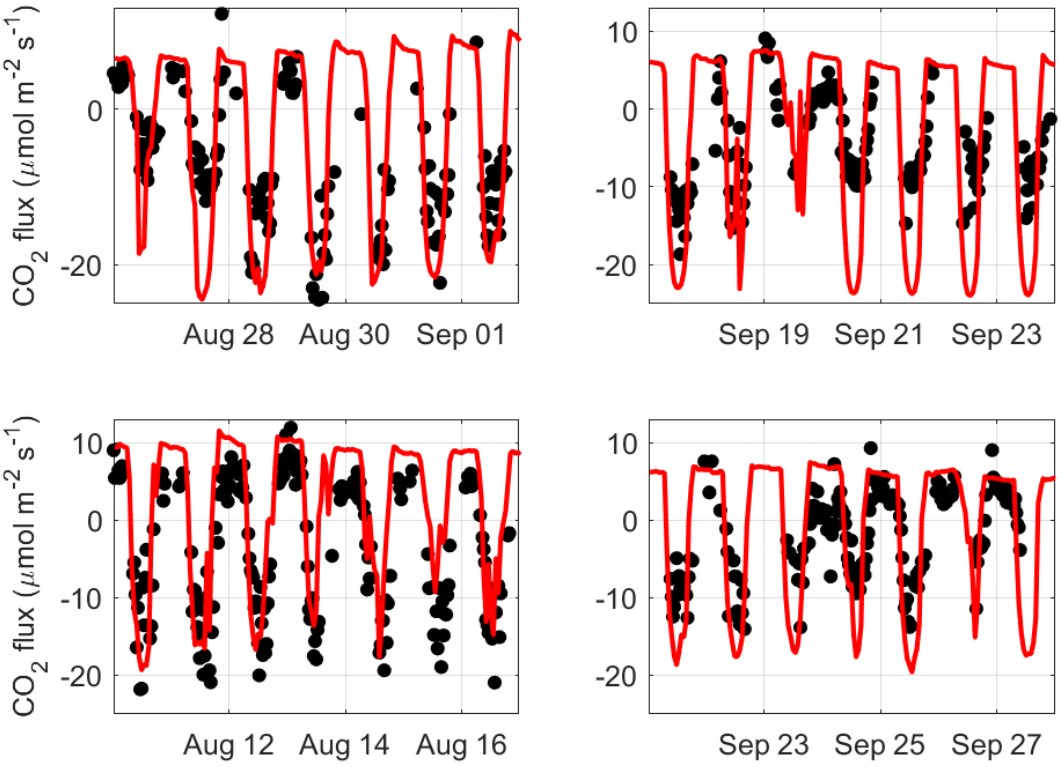

Figure 5. Modeled (red lines) and observed (black dots) CO_2 fluxes for four arbitrary weeklong periods in (a) August of 2015 (1.33 m water depth), (b) September of 2015 (1.40 m water depth), (c) August of 2016 (1.34 m water depth), (d) September of 2016 (1.36 m water depth).

Table 1. Goodness-of-fit metrics for modeled hourly CO_2 and CH_4 fluxes during the combined 2015 and 2016 growing seasons. All models were significant at $p < 0.0001$. Uncertainty estimated according to Hollinger and Richardson (2005).

Variable	Period	r^2	Observation Uncertainty	RMSD	Bias	Slope
		--	μmol m^{-2} s^{-1}	μmol m^{-2} s^{-1}	μmol m^{-2} s^{-1}	--
CO_2 Flux	All	0.54	3.35	7.30	-0.32	1.06
	2015	0.51	3.31	8.57	-1.46	1.16
	2016	0.56	3.36	6.67	0.08	1.01
CH_4 Flux	All	0.24	0.32	0.45	0.04	0.51
	2015	0.22	0.36	0.44	0.01	0.35
	2016	0.45	0.29	0.45	0.05	0.65

Ecosys simulations matched the observed hourly CO_2 fluxes well (Table 1; Figure 5). In general, the modeled CO_2 fluxes tended to underestimate early colder season fluxes but was closer to reality during the summer months. The *ecosys* modeled hourly CH_4 fluxes are considerably less variable than our observations (Figure 6), indicating uncertainties in model prediction methodologies. The disparities between the modeled and observed hourly CH_4 fluxes could be for many possible reasons due to the complexity of processes responsible for creating and transporting CH_4. If the highly variable eddy covariance methane fluxes are taken to be true data and not data noise, in principle the disparity must be attributable to differences in microbiological activity rates or due to transport processes. Biological activity, though, responds slowly to changes in soil and meteorological conditions, and so this seems an unlikely reason for highly variable hourly fluxes. On the other hand, transport processes can be quite variable in wetlands with standing water due to bubble emissions or turbulent transport of dissolved gases through the water column, both of which are fluxes that can respond quickly to changes in conditions. Although a bubble formulation is included in *ecosys*, the effect of water turbulence on increasing solute diffusion in the standing surface water is not explicitly modeled in *ecosys* (or any other major model) at present. The representation of water eddies in the model would hasten surface degassing when eddies are rising, and suppress it when they are descending, increasing temporal variation. This is potentially a very important pathway to model in order to describe marsh wetland surface-fluxes of methane since water turbulence leads to increased O_2 uptake and will facilitate CO_2 and CH_4 effluxes by reducing the diffusive resistance in the water column. Beyond these two mechanistic reasons why a disparity may exist, a third potential reason for disparities between observed and modeled CH_4 fluxes is that measured CH_4 fluxes

may have high error at present, and so it's not clear what level of variability is due to true ecosystem dynamics and how much is due to sensor noise.

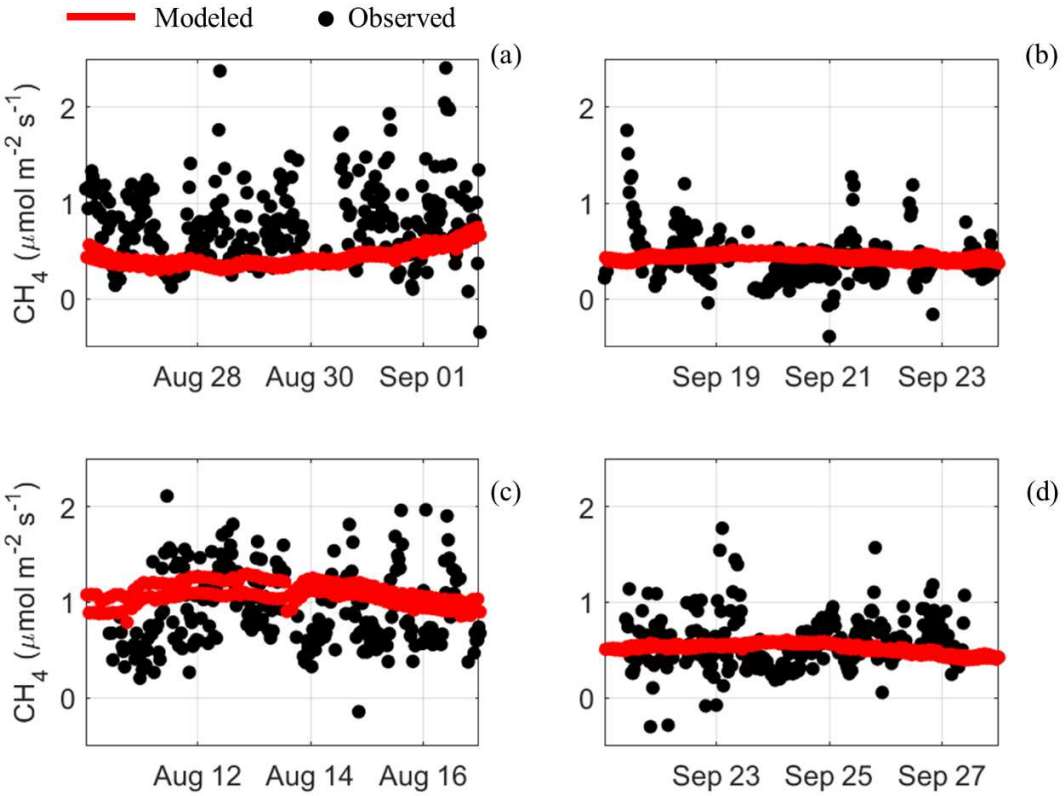

Figure 6.Modeled (red lines) and observed (black dots) CH_4 fluxes for four arbitrary weeklong periods in (a) August of 2015 (1.33 m water depth), (b) September of 2015 (1.40 m water depth), (c) August of 2016 (1.34 m water depth), (d) September of 2016 (1.36 m water depth). While CH_4 fluxes match the general trend, modeled CH_4 fluxes are far less variable than the half hour measurements of CH_4 observed by the EC tower.

For all these reasons, at present it makes a great deal of sense to compare CH_4 surface-fluxes on a daily scale over a season that to look at hourly fluxes. The model was able to reproduce the seasonal trends (Figure 7) (Table 2), similar to other process based model studies which were able to reproduce the seasonal trend of methane fluxes but not the daily or intra-daily fluctuations (Van Huissteden et al., 2008). While this method dampens our ability to predict the hour to hour flux, the annual budget is determined more by the day-to-day trend, which is considerably less random. Aggregating half hourly CH_4 fluxes to the daily scale, we can demonstrate that our model can properly predict the order of magnitude of the fluxes (Figure 7), which follow a predictable seasonal pattern. Modeled early season fluxes remain low because methanogenic biomass was small and aqueous CH_4 accumulates with greater solubility in the cooler soil water. Modelled fluxes then increase with seasonal warming as methanogenic

biomass grows and warmer soil water lowers CH_4 solubility, leading to aqueous CH_4 concentrations reaching saturationand causing bubbling.

Table 2. Goodness-of-fit metrics for modeled daily CH_4 fluxes during the combined 2015 and 2016 growing seasons. All models were significant at $p < 0.0001$.

Variable	Period	r^2	RMSD	Bias	Slope
		--	µmol m^{-2} s^{-1}	µmol m^{-2} s^{-1}	--
CH_4 Flux	All	0.27	0.43	0.13	0.67
	2015	0.43	0.4	0.01	0.70
	2016	0.19	0.45	0.26	0.72

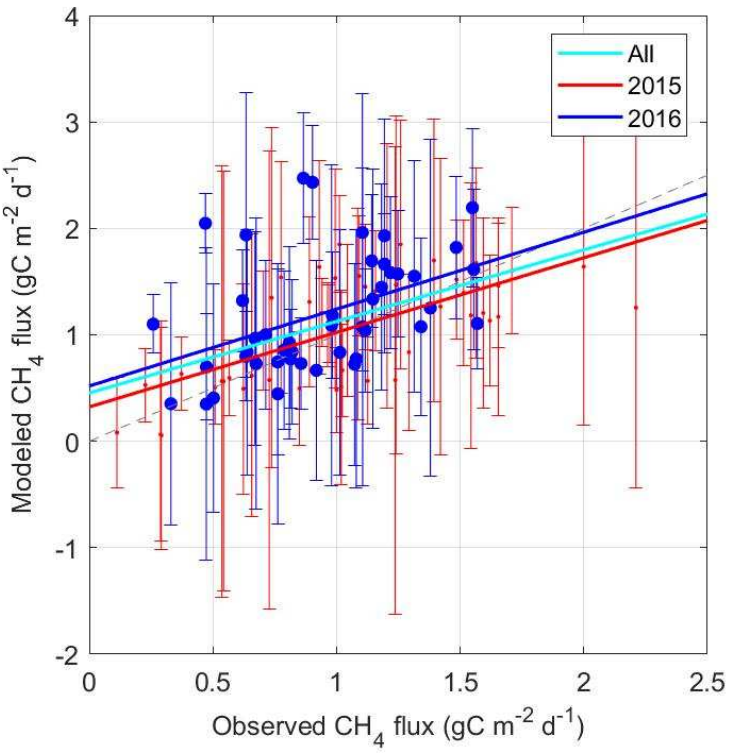

Figure 7. Observed and modeled daily averaged CH_4 flux. Grey dotted line indicates 1:1 line. Ecosys tended to overestimate CH_4 fluxes at the site, but maintained slopes near 1. Uncertainties are the average observation and gap-filling uncertainties for from hourly CH_4 flux uncertainties at the hourly level. Since the hourly flux uncertainty is so high, CH_4 fluxes are better compared at the daily level, where the aggregated uncertainties may cancel out to a degree.

Both the eddy covariance and model show high wavelet coherence at the seasonal time scales (2048 to 4096 hour periodicity, ~2.5-5 months), indicating that the model captures the CH_4 flux dynamics at the seasonal level quite well (Figure 8). However, the model and observations disagree on the phase angle between the two at nearly all lower periodicities by nearly 90°. This means that the model and observed values agree with one another regarding the relevant time spans that the two data signals agree, but they disagree on any kind of phase lag between them by approximately a quarter of a period. Although *ecosys* captures some coherence at lower periodicities (daily-weekly), the coherence is not as strong as was observed, indicating that events at those periodicities are not well represented by the model at this site.

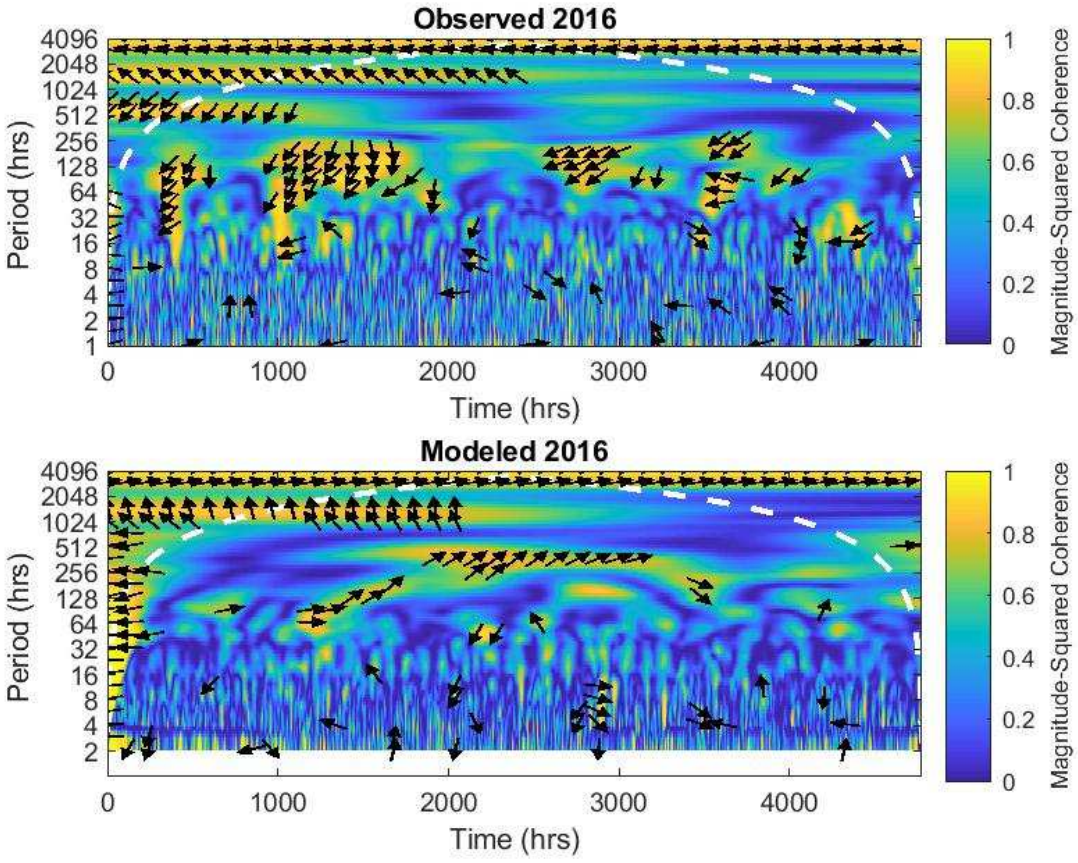

Figure 8. Wavelet coherence between water depth and CH_4 fluxes at OWC. Magnitude-squared coherence indicates strength of frequency co-spectral agreement, with values close to one being the strongest agreement and those near zero being the weakest. Arrow direction indicates the lag of agreement, where arrows pointed directly right are have aligned periodicity. Arrows pointed left have periods opposite one another (e.g. peaks in one variable align to troughs in the other). Both observations and the model show strong coherence at seasonal scale periodicities (higher than 2048 h), especially in 2015, but the phase angle between the two are off by nearly 90° at all periodicities, indicating that the phase lag is off by approximately a quarter of a period. Shorter time scales show weaker agreement.

3.5 Projections of wetland CO_2 fluxes

The four modeled 21st century OWC water-level scenarios had moderate effects on model projected CO_2 fluxes as long as the site remained flooded (Figure 9 a and b). In general, macrophyte vegetation in the model responded to rising temperatures by increasing productivity and increased soil nutrient availability, making the vegetated patch, and the wetland overall, an increasing sink for carbon in all other scenarios (Figure 9 a and b). However, most water level scenarios had only small effects on the CO_2 uptake strength of the wetland.

When aggregated to the site level (Figure 9b), the CO_2 fluxes from the LEWL1, LEWL2, and LEWL3 scenarios are similar but differ from the LEWL4 scenario. A greater portion of the wetland was available for plant colonization in the low water-level runs (Figure 3), slightly increasing the strength of the carbon uptake of the wetland under decreasing water depth scenarios (with the exception of LEWL4, which had a more complex response). High water-level conditions caused a smaller portion of the wetland to be available for plant colonization, but the plants were better adapted to the flooded conditions and thrived under the wetter conditions. In general, lower water depths increased wetland carbon uptake until the wetland dried out, which caused a substantial loss in the stored ecosystem carbon to the atmosphere.

LEWL4, the lowest water-level scenario, showed the greatest inter-annual variability in CO_2 fluxes. The LEWL4 scenario, where standing water had diminished by the last decade of the simulation, showed a sudden and sustained transition to a net ecosystem source of carbon as the water dried out. The modeled open-water grid cell was almost always a modest carbon source, indicating that uptake by submerged aquatic vegetation was more than offset by respiration, where the additional substrate carbon necessary to retain this source behavior was laterally transported from the vegetated grid cell.

In the LEWL4 scenario, broadleaf trees were established in year 2044, when the wetland water depth was at its lowest. In that model run, the trees became the dominant vegetation type after the wetland had lost its standing water. Trees were able to grow in the vegetated grid cell, but they only slowly colonized the deeper open water grid cell. The forested former wetland fluctuated shifted towards becoming a carbon source as the vegetation regime switched dominance and greater amounts of soil carbon were oxidized. Given a sustained runtime in this state, the former wetland likely would have become an even greater carbon sink due to wood C accumulation, however, it would have lost a great deal of carbon from its organic layers while stabilizing to that functionality.

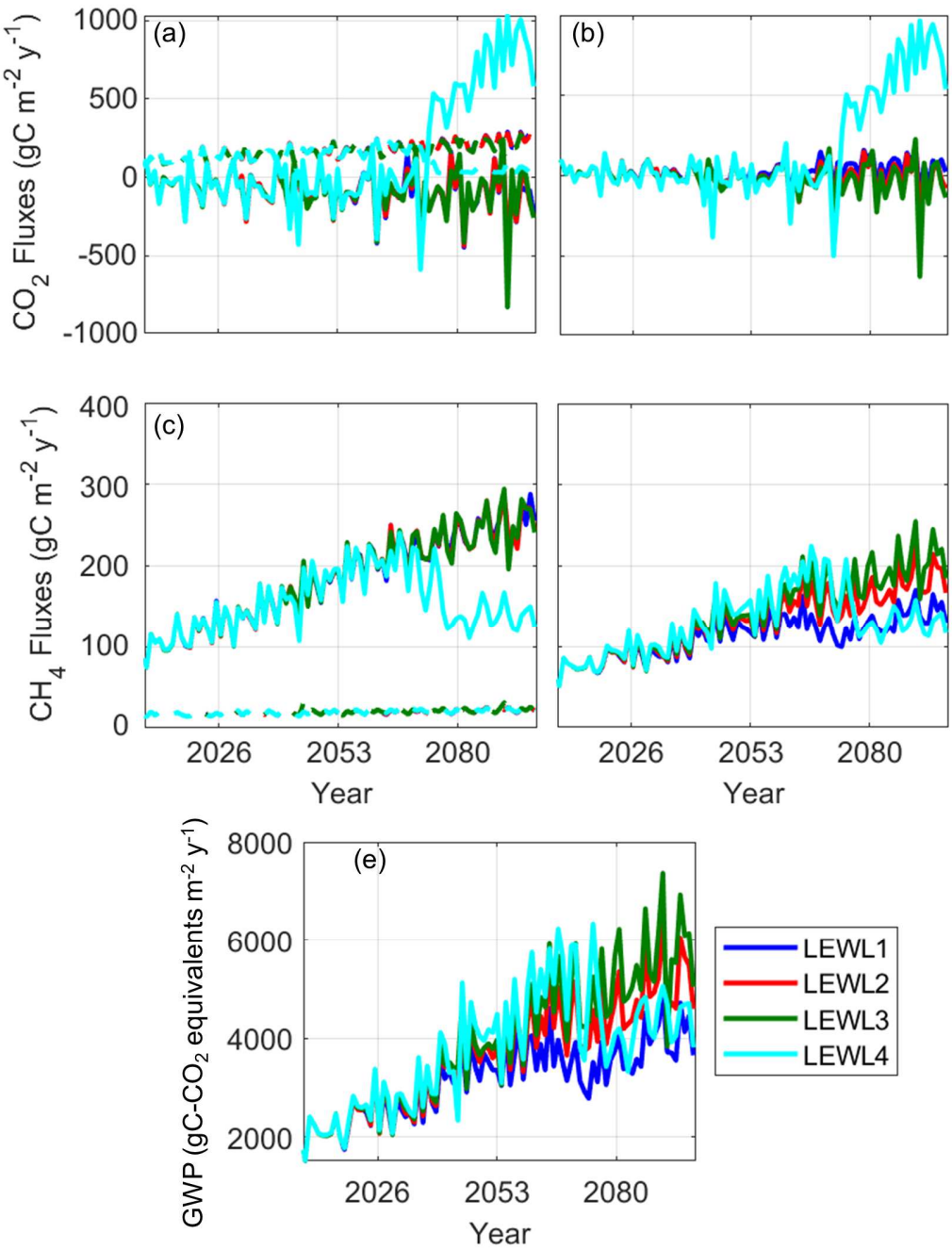

Figure 9. (a) CO_2 fluxes from vegetated (solid lines) and open water (dashed lines) grid cells for the model (negative values indicate net ecosystem uptake). In three of the four scenarios the open water CO_2 fluxes are small and slightly negative (those three scenarios are indistinguishable below the green dashed line). (b) Those same fluxes aggregated to the site footprint level using the projected footprint. (c) CH_4 fluxes from vegetated (solid lines) and the open water (dashed lines) grid cells for the model. In three of the four scenarios (LEWL 1-3) the open water fluxes are projected to remain positive to the atmosphere. The final scenario (LEWL4 based on a large drawdown of Lake Erie and a subsequently large drawdown of OWC) indicates a shift towards higher inter-annually variability, and lower decadal average, CH_4 fluxes. (d) Those same fluxes scaled to the site level using expected footprint distribution. In general, lower water depths slightly increased CH_4 fluxes, primarily by shifting terrain towards vegetated cover.

Both the lowest water depth scenario (LEWL4) and the highest water depth scenario (LEWL1) results in considerably lower CH_4 fluxes to the atmosphere due to lower emissions from the vegetated cell (LEWL4) or a higher areal cover of the open water cell (LEWL1). (e) Global warming potential of OWC projected over the 21st century. The OWC site remains a net GHG source under all projections. CH_4 fluxes can affect the overall GWP of the site, suggesting that a rapid drying of the wetland can result in large decreases in this source behavior (illustrated by LEWL4)). Increased water depth moderates source behavior by limiting the areal percent of the wetland that can support vegetation which can lower CH_4 emissions and bring down the overall site level CH_4 fluxes (illustrated by LEWL1).

3.6 Sensitivity of CH_4 fluxes to predicted future lake water depths

We found that CH_4 fluxes also showed relatively low sensitivity to water depth in three of the four scenarios (Figure 9 c and d), with the three wettest scenarios showing close agreement in projected CH_4 fluxes in most years. This result agrees well with Figure 8, which indicates a linkage between fluxes and water depth fluctuations, but with the strongest linkages are at multi-daily time scales. However, we found the relationship between the modeled water depth and the modeled CH_4 fluxes was significant on an annual basis (Figure 10 d), but with a negative slope. The negative slope indicates that as water depth increases the CH_4 fluxes generally decrease due to the reduction of primary productivity, and thus litterfall from which the model drives the heterotrophic fermentation rates that produces methanogenic substrates. The relationship between these two variables is non-linear though, where very low water levels can exhibit a wide range of CH_4 fluxes while deeper water exhibits a much more linear control on the emissions. Similar to the results in the open water and vegetated grid cells, the aggregated site-level CH_4 fluxes in the three wet runs remain close in magnitude (Figure 9 c). We also found that drying events, as presented in one of our water depth scenarios, can cause both decreases in CH_4 fluxes and a switch from a CO_2 sink to a CO_2 source as oxygen infiltrates the soil. In LEWL4, for instance, when the surface vegetation changed dramatically, both CO_2 and CH_4 fluxes responded accordingly. We projected a decrease in cumulative CH_4 fluxes from a peak of 224.6 in 2067 to 104.7 gC m^{-2} $year^{-1}$ 2083. In that same time period, we projected CO_2 flux changed from -56.5 gC m^{-2} $year^{-1}$ to 396.6 gC m^{-2} $year^{-1}$. It should be noted that the fluxes at OWC are large compared to similar systems and have been cited as an outlier in FLUXNET synthesis studies such as in (2019), where OWC is cited as the highest magnitude fluxes. Although freshwater marshes were cited as having the largest fluxes of any wetland ecotype with a median flux of 43.2 gC m^{-2} y^{-1}, OWC was cited as having fluxes of ~115 gC m^{-2} $year^{-1}$.

However, when accounting for the variability of the site plant community structure the scenarios more starkly diverge (Figure 9d), due to the greater difference between CH_4 fluxes from the open water and vegetated grid-cells. The fluxes rapidly decreased when surface water drained with declining water depth. This decrease is also indicated in the regression between CH_4 fluxes and water depths which is apparent when water depths are very low (primarily associated with LEWL4). This variability at low water levels is counter to the relationship between water depth and CH_4 fluxes when the water is deeper, but is

explained by the introduction of oxygen and hence methanotrophy into the near-surface soil. Our model predictions are generally in line with observational studies that suggest that the presence of surface water strongly regulates CH_4 fluxes (Grünfeld and Brix, 1999; Meijide et al., 2011; Pypker et al., 2013; Sturtevant et al., 2011; Zona et al., 2009). When sufficiently wet, the soil supports methanogenic activity due to the low soil oxygen levels and when soil dries out, methanogenesis decreases and methanotrophy increases.

We also found that the integrated leaf area index (i.e. the footprint weighted LAI between the two cells) was significantly related to CH_4 fluxes (Figure 10c), indicating that the plant productivity is a strong driver of CH_4 fluxes. Our findings are also consistent with Turetsky et al. (2014), who found that CH_4 fluxes from rich fens respond dramatically to changes in surface vegetation. Our combined models suggest that one of the primary ways in which water level can affect site level methane emissions is by controlling the surface vegetation community.

Our projections of wetland CH_4 fluxes are generally consistent with those in other modeling studies which suggest that wetland CH_4 fluxes will increase in a warming climate (Cao et al., 1998; Gedney et al., 2004). Measured CH_4 emissions have been found to have a large apparent Q10, and those models simulate this response through a combination of physical and biological processes. Those same models indicate that drying soils can potentially lower methane emissions due to increased methanotrophy. Gedney et al. (2004) forecasted that wetlands would experience a GWP increase of 5-10% by 2100 due to increased temperatures alone, for instance. Our model suggests a greater increase: closer to 50% by 2100 for the LEWL scenarios that projected water levels closest to present day (i.e. LEWL2 and LEWL3). A very large percent of that increase is due to the increase in methane emissions, which are already quite high for OWC.

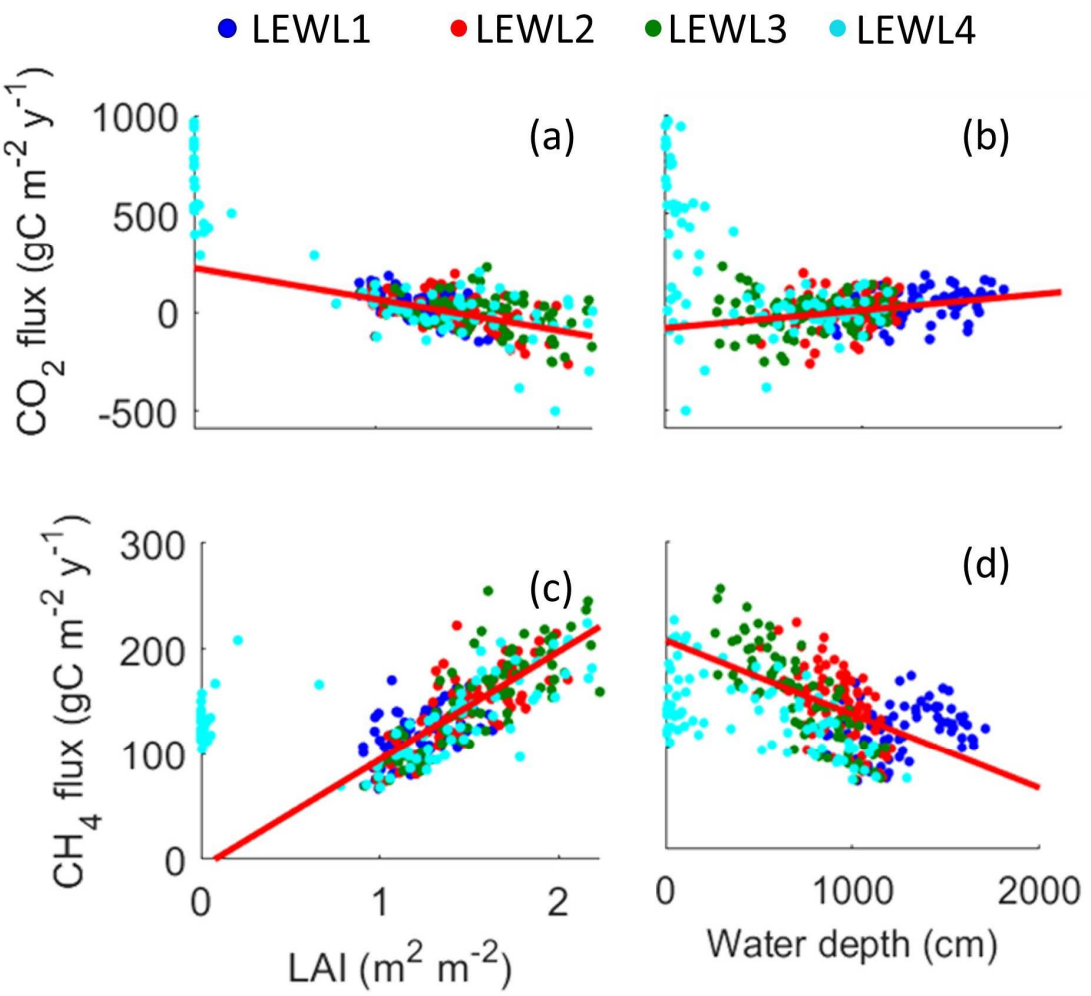

Figure 10. Annual modeled fluxes of CO_2 and CH_4 fluxes vs peak annual LAI and mean annual water depth. Lack of water in LEWL4 causes highly non-linear effects and so was disregarded for the regressions shown here to emphasize influence of water level variations when flooded. All four relationships were significant ($p<0.05$). Substantial drained time with belowground water tables (i.e. even longer than we simulated here in LEWL4) may alter this relationship as methanotrophy increases and new PFTs take hold.

4. Conclusions

Shifts in the water depths of the Great Lakes may have major implications for carbon cycling of neighboring lacustrine wetlands, especially since the range of water depth scenarios includes situations that could result in moderate drying of these wetlands. Shifts in vegetation composition from long-term water depth changes may affect wetland function and greenhouse gas budgets. We found that the relative areas of the vegetated and non-vegetated grid-cells played important roles in determining the wetland CO_2 and CH_4 fluxes, and correspondingly the total global-warming potential of the site (Figure 9 e). The vegetated grid-cell maintains higher magnitudes of both CO_2 and CH_4 fluxes than non-vegetated grid-cells. We found that reduction in water depths sufficient to dry portions of the wetland resulted in woody

vegetation colonizing the former wetland area, which fundamentally altered ecosystem nutrient and carbon cycling.

In all scenarios, warming climate leads to increased plant productivity and greater CH_4 fluxes. Under three of the four projections of Lake Erie water depths, CO_2 and CH_4 fluxes increase steadily over the 21st century in response primarily to the increasing temperatures. However, in situations where the standing water recedes and the soil becomes more aerobic the soil conditions become less suitable for methanogenesis and more suitable for microbial and root respiration. Our model therefore predicts that areas that were previously strong CH_4 sources will have decreased CH_4 fluxes and increased CO_2 fluxes (both respiration and uptake) as non-wetland plant functional types colonize the wetland. However, the majority of predicted water-level scenarios resulted in maintaining or increasing current net carbon sequestration levels, with the wetlands continuing to serve as atmospheric CO_2 sinks and CH_4 sources.

5. Code availability

The exact version of the model used to produce the results in this paper is archived on a Dataverse repository, as are input data for all the simulations presented in this paper.

6. Data availability

The data that the model was validated against were obtained from Ameriflux,(site code US-OWC). They are archived with the model run on a Dataverse repository.

7. Acknowledgements

This study was supported by the Ohio Water Development Authority (award 7880), Ohio Water Resources Research Center (award G16AP00076), a NOAA Davidson Fellowship (NA18NOS42000079) administered by ODNR through OWC-NERR (Subaward N18B 315-11), and the US Department of Energy (awards DE-SC0022191, DE-SC0021067, and Graduate Research Program, Solicitation-2 Fellowship to THM). Funding for flux data collection at US-OWC, part of the UMBS AmeriFlux core site cluster, was provided in part by the U.S. Department of Energy's Office of Science. Site access, meteorology and water observations, and technical support were provided by Kristin Arend and the OWC management team (NERR/NOAA/ODNR). WJR was supported by the Director, Office of Science, Office of Biological and Environmental Research of the US Department of Energy under contract no. DE-AC02-05CH11231 to Lawrence Berkeley National Laboratory as part of the RUBISCO Scientific Focus Area.

8. References

Amthor, J. S., Chen, J. M., Clein, J. S., Frolking, S. E., Goulden, M. L., Grant, R. F., Kimball, J. S., King, A. W., McGuire, A. D., Nikolov, N. T., Potter, C. S., Wang, S., and Wofsy, S. C.: Boreal forest CO2 exchange and evapotranspiration predicted by nine ecosystem process models: Intermodel comparisons and relationships to field measurements, 106, 33623–33648, https://doi.org/10.1029/2000JD900850, 2001.

Angle, J. C., Morin, T. H., Solden, L. M., Narrowe, A. B., Smith, G. J., Borton, M. A., Rey-Sanchez, C., Daly, R. A., Mirfenderesgi, G., Hoyt, D. W., Riley, W. J., Miller, C. S., Bohrer, G., and Wrighton, K. C.: Methanogenesis in oxygenated soils is a substantial fraction of wetland methane emissions, 8, 1567, https://doi.org/10.1038/s41467-017-01753-4, 2017.

Armstrong, W.: Aeration in Higher Plants, in: Advances in Botanical Research, vol. 7, edited by: Woolhouse, H. W., Academic Press, 225–332, https://doi.org/10.1016/S0065-2296(08)60089-0, 1980.

Bernal, B. and Mitsch, W. J.: A comparison of soil carbon pools and profiles in wetlands in Costa Rica and Ohio, Ecological Engineering, 34, 311–323, https://doi.org/10.1016/j.ecoleng.2008.09.005, 2008.

Bohrer, G., Kerns, J., Morin, T. H., Rey-Sanchez, A. C., Villa, J. A., and Ju, Y.: AmeriFlux US-OWC Old Woman Creek, Dataset, https://doi.org/10.17190/AMF/1418679, 2015.

Bohrer, G., Ju, Y., Arend, K., Morin, T. H., Rey-Sanchez, A. C., Wrighton, K. C., and Villa, J. A.: Methane and CO2 chamber fluxes and porewater concentrations US-OWC Ameriflux wetland site, 2015-2018. AmeriFlux Management Project, edited by ESS-DiVE, https://doi.org/doi:10.15485/1568865, 2019.

Cao, M., Gregson, K., and Marshall, S.: Global methane emission from wetlands and its sensitivity to climate change, Atmospheric Environment, 32, 3293–3299, https://doi.org/10.1016/S1352-2310(98)00105-8, 1998.

Casanova, M. T. and Brock, M. A.: How do depth, duration and frequency of flooding influence the establishment of wetland plant communities?, Plant Ecology, 147, 237–250, https://doi.org/10.1023/A:1009875226637, 2000.

Chang, K.-Y., Riley, W. J., Brodie, E. L., McCalley, C. K., Crill, P. M., and Grant, R. F.: Methane Production Pathway Regulated Proximally by Substrate Availability and Distally by Temperature in a High-Latitude Mire Complex, 124, 3057–3074, https://doi.org/10.1029/2019JG005355, 2019.

Chang, K.-Y., Riley, W. J., Crill, P. M., Grant, R. F., and Saleska, S. R.: Hysteretic temperature sensitivity of wetland CH_4 fluxes explained by substrate availability and microbial activity, 17, 5849–5860, https://doi.org/10.5194/bg-17-5849-2020, 2020.

Colmer, T. D.: Long-distance transport of gases in plants: a perspective on internal aeration and radial oxygen loss from roots, 26, 17–36, https://doi.org/10.1046/j.1365-3040.2003.00846.x, 2003.

Detto, M., Montaldo, N., Albertson, J. D., Mancini, M., and Katul, G.: Soil moisture and vegetation controls on evapotranspiration in a heterogeneous Mediterranean ecosystem on Sardinia, Italy, 42, https://doi.org/10.1029/2005WR004693, 2006.

Detto, M., Verfaillie, J., Anderson, F., Xu, L., and Baldocchi, D.: Comparing laser-based open- and closed-path gas analyzers to measure methane fluxes using the eddy covariance method, Agricultural and Forest Meteorology, 151, 1312–1324, https://doi.org/10.1016/j.agrformet.2011.05.014, 2011.

Dietze, M. C., Vargas, R., Richardson, A. D., Stoy, P. C., Barr, A. G., Anderson, R. S., Arain, M. A., Baker, I. T., Black, T. A., Chen, J. M., Ciais, P., Flanagan, L. B., Gough, C. M., Grant, R. F., Hollinger, D., Izaurralde, R. C., Kucharik, C. J., Lafleur, P., Liu, S., Lokupitiya, E., Luo, Y., Munger, J. W., Peng, C., Poulter, B., Price, D. T., Ricciuto, D. M., Riley, W. J., Sahoo, A. K., Schaefer, K., Suyker, A. E., Tian, H., Tonitto, C., Verbeeck, H., Verma, S. B., Wang, W., and Weng, E.: Characterizing the performance of ecosystem models across time scales: A spectral analysis of the North American Carbon Program site-level synthesis, 116, https://doi.org/10.1029/2011JG001661, 2011.

Dimitrov, D. D., Bhatti, J. S., and Grant, R. F.: The transition zones (ecotone) between boreal forests and peatlands: Ecological controls on ecosystem productivity along a transition zone between upland black spruce forest and a poor forested fen in central Saskatchewan, Ecological Modelling, 291, 96–108, https://doi.org/10.1016/j.ecolmodel.2014.07.020, 2014a.

Dimitrov, D. D., Bhatti, J. S., and Grant, R. F.: The transition zones (ecotone) between boreal forests and peatlands: Modelling water table along a transition zone between upland black spruce forest and poor forested fen in central Saskatchewan, Ecological Modelling, 274, 57–70, https://doi.org/10.1016/j.ecolmodel.2013.11.030, 2014b.

Elberling, B., Askaer, L., Jørgensen, C. J., Joensen, H. P., Kühl, M., Glud, R. N., and Lauritsen, F. R.: Linking Soil O2, CO2, and CH4 Concentrations in a Wetland Soil: Implications for CO2 and CH4 Fluxes, Environ. Sci. Technol., 45, 3393–3399, https://doi.org/10.1021/es103540k, 2011.

Eyring, V., Bony, S., Meehl, G. A., Senior, C. A., Stevens, B., Stouffer, R. J., and Taylor, K. E.: Overview of the Coupled Model Intercomparison Project Phase 6 (CMIP6) experimental design and organization, 9, https://doi.org/10.5194/gmd-9-1937-2016, 2016.

Garnet, K. N., Megonigal, J. P., Litchfield, C., and Taylor, G. E.: Physiological control of leaf methane emission from wetland plants, Aquatic Botany, 81, 141–155, https://doi.org/10.1016/j.aquabot.2004.10.003, 2005.

Gedney, N., Cox, P. M., and Huntingford, C.: Climate feedback from wetland methane emissions, 31, https://doi.org/10.1029/2004GL020919, 2004.

Grant, R. F.: Changes in Soil Organic Matter under Different Tillage and Rotation: Mathematical Modeling in ecosys, 61, 1159–1175, https://doi.org/10.2136/sssaj1997.03615995006100040023x, 1997.

Grant, R. F.: Modelling changes in nitrogen cycling to sustain increases in forest productivity under elevated atmospheric CO2 and contrasting site conditions, Biogeosciences, 10, 7703–7721, https://doi.org/10.5194/bg-10-7703-2013, 2013.

Grant, R. F. and Roulet, N. T.: Methane efflux from boreal wetlands: Theory and testing of the ecosystem model Ecosys with chamber and tower flux measurements, 16, 2-1-2–16, https://doi.org/10.1029/2001GB001702, 2002.

Grant, R. F., Black, T. A., Hartog, G. den, Berry, J. A., Neumann, H. H., Blanken, P. D., Yang, P. C., Russell, C., and Nalder, I. A.: Diurnal and annual exchanges of mass and energy between an aspen-hazelnut forest and the atmosphere: Testing the mathematical model Ecosys with data from the BOREAS experiment, 104, 27699–27717, https://doi.org/10.1029/1998JD200117, 1999.

Grant, R. F., Desai, A. R., and Sulman, B. N.: Modelling contrasting responses of wetland productivity to changes in water table depth, 9, 5579–5623, https://doi.org/10.5194/bgd-9-5579-2012, 2012.

Grant, R. F., Mekonnen, Z. A., Riley, W. J., Wainwright, H. M., Graham, D., and Torn, M. S.: Mathematical Modelling of Arctic Polygonal Tundra with Ecosys: 1. Microtopography Determines How Active Layer Depths Respond to Changes in Temperature and Precipitation, 122, 3161–3173, https://doi.org/10.1002/2017JG004035, 2017a.

Grant, R. F., Mekonnen, Z. A., Riley, W. J., Arora, B., and Torn, M. S.: Mathematical Modelling of Arctic Polygonal Tundra with Ecosys: 2. Microtopography Determines How CO2 and CH4 Exchange Responds to Changes in Temperature and Precipitation, 122, 3174–3187, https://doi.org/10.1002/2017JG004037, 2017b.

Grünfeld, S. and Brix, H.: Methanogenesis and methane emissions: effects of water table, substrate type and presence of Phragmites australis, Aquatic Botany, 64, 63–75, https://doi.org/10.1016/S0304-3770(99)00010-8, 1999.

Hanson, P. J., Amthor, J. S., Wullschleger, S. D., Wilson, K. B., Grant, R. F., Hartley, A., Hui, D., Jr, E. R. H., Johnson, D. W., Kimball, J. S., King, A. W., Luo, Y., McNulty, S. G., Sun, G., Thornton, P. E., Wang, S., Williams, M., Baldocchi, D. D., and Cushman, R. M.: Oak Forest Carbon and Water Simulations: Model Intercomparisons and Evaluations Against Independent Data, 74, 443–489, https://doi.org/10.1890/03-4049, 2004.

Hatala, J. A., Detto, M., and Baldocchi, D. D.: Gross ecosystem photosynthesis causes a diurnal pattern in methane emission from rice, 39, https://doi.org/10.1029/2012GL051303, 2012.

Hollinger, D. Y. and Richardson, A. D.: Uncertainty in eddy covariance measurements and its application to physiological models, Tree Physiol, 25, 873–885, https://doi.org/10.1093/treephys/25.7.873, 2005.

Hsieh, C.-I., Katul, G., and Chi, T.: An approximate analytical model for footprint estimation of scalar fluxes in thermally stratified atmospheric flows, Advances in Water Resources, 23, 765–772, https://doi.org/10.1016/S0309-1708(99)00042-1, 2000.

Jeffrey, L. C., Maher, D. T., Johnston, S. G., Kelaher, B. P., Steven, A., and Tait, D. R.: Wetland methane emissions dominated by plant-mediated fluxes: Contrasting emissions pathways and seasons within a shallow freshwater subtropical wetland, 0, https://doi.org/10.1002/lno.11158, 2019.

Justin, S. H. F. W. and Armstrong, W.: The Anatomical Characteristics of Roots and Plant Response to Soil Flooding, 106, 465–495, 1987.

Kao-Kniffin, J., Freyre, D. S., and Balser, T. C.: Methane dynamics across wetland plant species, Aquatic Botany, 93, 107–113, https://doi.org/10.1016/j.aquabot.2010.03.009, 2010.

Keddy, P. A. and Ellis, T. H.: Seedling recruitment of 11 wetland plant species along a water level gradient: shared or distinct responses?, Can. J. Bot., 63, 1876–1879, https://doi.org/10.1139/b85-263, 1985.

Knox, S. H., Jackson, R. B., Poulter, B., McNicol, G., Fluet-Chouinard, E., Zhang, Z., Hugelius, G., Bousquet, P., Canadell, J. G., Saunois, M., Papale, D., Chu, H., Keenan, T. F., Baldocchi, D., Torn, M. S., Mammarella, I., Trotta, C., Aurela, M., Bohrer, G., Campbell, D. I., Cescatti, A., Chamberlain, S., Chen, J., Chen, W., Dengel, S., Desai, A. R., Euskirchen, E., Friborg, T., Gasbarra, D., Goded, I., Goeckede, M., Heimann, M., Helbig, M., Hirano, T., Hollinger, D. Y., Iwata, H., Kang, M., Klatt, J., Krauss, K. W., Kutzbach, L., Lohila, A., Mitra, B., Morin, T. H., Nilsson, M. B., Niu, S., Noormets, A., Oechel, W. C., Peichl, M., Peltola, O., Reba, M. L., Richardson, A. D., Runkle, B. R. K., Ryu, Y., Sachs, T., Schäfer, K.

V. R., Schmid, H. P., Shurpali, N., Sonnentag, O., Tang, A. C. I., Ueyama, M., Vargas, R., Vesala, T., Ward, E. J., Windham-Myers, L., Wohlfahrt, G., and Zona, D.: FLUXNET-CH4 Synthesis Activity: Objectives, Observations, and Future Directions, Bull. Amer. Meteor. Soc., 100, 2607–2632, https://doi.org/10.1175/BAMS-D-18-0268.1, 2019.

Laan, P., Berrevoets, M. J., Lythe, S., Armstrong, W., and Blom, C. W. P. M.: Root Morphology and Aerenchyma Formation as Indicators of the Flood-Tolerance of Rumex Species, 77, 693–703, https://doi.org/10.2307/2260979, 1989.

Lee, X., Massman, W., and Law, B.: Handbook of Micrometeorology: A Guide for Surface Flux Measurement and Analysis, Springer Science & Business Media, 270 pp., 2004.

Lenssen, J., Menting, F., van der Putten, W., and Blom, K.: Control of Plant Species Richness and Zonation of Functional Groups along a Freshwater Flooding Gradient, 86, 523–534, https://doi.org/10.2307/3546656, 1999.

Lofgren, B. M., Hunter, T. S., and Wilbarger, J.: Effects of using air temperature as a proxy for potential evapotranspiration in climate change scenarios of Great Lakes basin hydrology, Journal of Great Lakes Research, 37, 744–752, https://doi.org/10.1016/j.jglr.2011.09.006, 2011.

Massman, W. J.: A simple method for estimating frequency response corrections for eddy covariance systems, Agricultural and Forest Meteorology, 104, 185–198, https://doi.org/10.1016/S0168-1923(00)00164-7, 2000.

Matheny, A. M., Bohrer, G., Stoy, P. C., Baker, I. T., Black, A. T., Desai, A. R., Dietze, M. C., Gough, C. M., Ivanov, V. Y., Jassal, R. S., Novick, K. A., Schäfer, K. V. R., and Verbeeck, H.: Characterizing the diurnal patterns of errors in the prediction of evapotranspiration by several land-surface models: An NACP analysis, 119, 1458–1473, https://doi.org/10.1002/2014JG002623, 2014.

Meehl, G. A., Boer, G. J., Covey, C., Latif, M., and Stouffer, R. J.: The Coupled Model Intercomparison Project (CMIP), 81, 313–318, 2000.

Meijide, A., Manca, G., Goded, I., Magliulo, V., Tommasi, P. di, Seufert, G., and Cescatti, A.: Seasonal trends and environmental controls of methane emissions in a rice paddy field in Northern Italy, 8, 3809–3821, https://doi.org/doi:10.5194/bg-8-3809-2011, 2011.

Mekonnen, Z. A., Grant, R. F., and Schwalm, C.: Sensitivity of modeled NEP to climate forcing and soil at site and regional scales: Implications for upscaling ecosystem models, Ecological Modelling, 320, 241–257, https://doi.org/10.1016/j.ecolmodel.2015.10.004, 2016.

Melton, J. R., Wania, R., Hodson, E. L., Poulter, B., RINGEVAL, B., Spahni, R., Bohn, T., Avis, C. A., Beerling, D. J., Chen, G., Eliseev, A. V., Denisov, S. N., Hopcroft, P. O., Lettenmaier, D. P., Riley, W. J., Singarayer, J. S., Subin, Z. M., Tian, H., Urcher, S. Z. ¨, Brovkin, V., van Bodegom, P. M., Kleinen, T., Yu, Z. C., and Kaplan, J. O.: Present state of global wetland extent and wetland methane modelling: conclusions from a model inter-comparison project (WETCHIMP), 10, 753–788, https://doi.org/10.5194/bg-10-753-2013, 2013.

Mezbahuddin, M., Grant, R. F., and Hirano, T.: Modelling effects of seasonal variation in water table depth on net ecosystem CO2 exchange of a tropical peatland, 11, 577–599, https://doi.org/10.5194/bg-11-577-2014, 2014.

Morin, T. H., Bohrer, G., Frasson, R. P. d M., Naor-Azreli, L., Mesi, S., Stefanik, K. C., and Schäfer, K. V. R.: Environmental drivers of methane fluxes from an urban temperate wetland park, 119, 2188–2208, https://doi.org/10.1002/2014JG002750, 2014a.

Morin, T. H., Bohrer, G., Naor-Azrieli, L., Mesi, S., Kenny, W. T., Mitsch, W. J., and Schäfer, K. V. R.: The seasonal and diurnal dynamics of methane flux at a created urban wetland, 72, 74–83, https://doi.org/10.1016/j.ecoleng.2014.02.002, 2014b.

Home | Centralized Data Management Office: http://cdmo.baruch.sc.edu/, last access: 3 June 2020.

Nowak, M., Beulig, F., von Fischer, J., Muhr, J., Küsel, K., and Trumbore, S. E.: Autotrophic fixation of geogenic CO2 by microorganisms contributes to soil organic matter formation and alters isotope signatures in a wetland mofette, 12, 7169–7183, https://doi.org/10.5194/bg-12-7169-2015, 2015.

Pachauri, R. K., Allen, M. R., Barros, V. R., Broome, J., Cramer, W., Christ, R., Church, J. A., Clarke, L., Dahe, Q., Dasgupta, P., Dubash, N. K., Edenhofer, O., Elgizouli, I., Field, C. B., Forster, P., Friedlingstein, P., Fuglestvedt, J., Gomez-Echeverri, L., Hallegatte, S., Hegerl, G., Howden, M., Jiang, K., Jimenez Cisneroz, B., Kattsov, V., Lee, H., Mach, K. J., Marotzke, J., Mastrandrea, M. D., Meyer, L., Minx, J., Mulugetta, Y., O'Brien, K., Oppenheimer, M., Pereira, J. J., Pichs-Madruga, R., Plattner, G.-K., Pörtner, H.-O., Power, S. B., Preston, B., Ravindranath, N. H., Reisinger, A., Riahi, K., Rusticucci, M., Scholes, R., Seyboth, K., Sokona, Y., Stavins, R., Stocker, T. F., Tschakert, P., van Vuuren, D., and van Ypserle, J.-P.: Climate Change 2014: Synthesis Report. Contribution of Working Groups I, II and III to the Fifth Assessment Report of the Intergovernmental Panel on Climate Change, edited by: Pachauri, R. K. and Meyer, L., IPCC, Geneva, Switzerland, 151 pp., 2014.

Poiani, K. A. and Johnson, W. C.: A Spatial Simulation Model of Hydrology and Vegetation Dynamics in Semi-Permanent Prairie Wetlands, 3, 279–293, https://doi.org/10.2307/1941831, 1993.

Poulter, B., Bousquet, P., Canadell, J. G., Ciais, P., Peregon, A., Saunois, M., Arora, V. K., Beerling, D. J., Brovkin, V., Jones, C. D., Joos, F., Gedney, N., Ito, A., Kleinen, T., Koven, C. D., McDonald, K., Melton, J. R., Peng, C., Peng, S., Prigent, C., Schroeder, R., Riley, W. J., Saito, M., Spahni, R., Tian, H., Taylor, L., Viovy, N., Wilton, D., Wiltshire, A., Xu, X., Zhang, B., Zhang, Z., and Zhu, Q.: Global wetland contribution to 2000–2012 atmospheric methane growth rate dynamics, Environ. Res. Lett., 12, 094013, https://doi.org/10.1088/1748-9326/aa8391, 2017.

Pypker, T., Moore, P., Hribljan, J., and Chimner, R.: Shifting environmental controls on CH4 fluxes in a sub-boreal peatland, 10, 7971–7981, https://doi.org/10.5194/bg-10-7971-2013, 2013.

Rawls, W. J., Brakensiek, D. L., and Saxtonn, K. E.: Estimation of Soil Water Properties, 25, 1316–1320, https://doi.org/10.13031/2013.33720, 1982.

Reichstein, M., Falge, E., Baldocchi, D., Papale, D., Aubinet, M., Berbigier, P., Bernhofer, C., Buchmann, N., Gilmanov, T., Granier, A., Grünwald, T., Havránková, K., Ilvesniemi, H., Janous, D., Knohl, A., Laurila, T., Lohila, A., Loustau, D., Matteucci, G., Meyers, T., Miglietta, F., Ourcival, J.-M., Pumpanen, J., Rambal, S., Rotenberg, E., Sanz, M., Tenhunen, J., Seufert, G., Vaccari, F., Vesala, T., Yakir, D., and Valentini, R.: On the separation of net ecosystem exchange into assimilation and ecosystem respiration: review and improved algorithm, 11, 1424–1439, https://doi.org/10.1111/j.1365-2486.2005.001002.x, 2005.

Rey-Sanchez, A. C., Morin, T. H., Stefanik, K. C., Wrighton, K., and Bohrer, G.: Determining total emissions and environmental drivers of methane flux in a Lake Erie estuarine marsh, Ecological Engineering, 114, 7–15, https://doi.org/10.1016/j.ecoleng.2017.06.042, 2018.

Saunois, M., Stavert, A. R., Poulter, B., Bousquet, P., Canadell, J. G., Jackson, R. B., Raymond, P. A., Dlugokencky, E. J., Houweling, S., Patra, P. K., Ciais, P., Arora, V. K., Bastviken, D., Bergamaschi, P., Blake, D. R., Brailsford, G., Bruhwiler, L., Carlson, K. M., Carrol, M., Castaldi, S., Chandra, N., Crevoisier, C., Crill, P. M., Covey, K., Curry, C. L., Etiope, G., Frankenberg, C., Gedney, N., Hegglin, M. I., Höglund-Isaksson, L., Hugelius, G., Ishizawa, M., Ito, A., Janssens-Maenhout, G., Jensen, K. M., Joos, F., Kleinen, T., Krummel, P. B., Langenfelds, R. L., Laruelle, G. G., Liu, L., Machida, T., Maksyutov, S., McDonald, K. C., McNorton, J., Miller, P. A., Melton, J. R., Morino, I., Müller, J., Murgia-Flores, F., Naik, V., Niwa, Y., Noce, S., O'Doherty, S., Parker, R. J., Peng, C., Peng, S., Peters, G. P., Prigent, C., Prinn, R. G., Ramonet, M., Regnier, P., Riley, W. J., Rosentreter, J. A., Segers, A., Simpson, I. J., Shi, H., Smith, S. J., Steele, L. P., Thornton, B. F., Tian, H., Tohjima, Y., Tubiello, F. N., Tsuruta, A., Viovy, N., Voulgarakis, A., Weber, T. S., Weele, M. van, Werf, G. R. van der, Weiss, R. F., Worthy, D., Wunch, D., Yin, Y., Yoshida, Y., Zhang, W., Zhang, Z., Zhao, Y., Zheng, B., Zhu, Q., Zhu, Q., and Zhuang, Q.: The Global Methane Budget 2000-2017, 2019.

Saxton, K. E. and Rawls, W. J.: Soil Water Characteristic Estimates by Texture and Organic Matter for Hydrologic Solutions, 70, 1569–1578, https://doi.org/10.2136/sssaj2005.0117, 2006.

Seabloom, E. W., van der Valk, A. G., and Moloney, K. A.: The role of water depth and soil temperature in determining initial composition of prairie wetland coenoclines, Plant Ecology, 138, 203–216, https://doi.org/10.1023/A:1009711919757, 1998.

Seabloom, E. W., Moloney, K. A., and Valk, A. G. van der: Constraints on the Establishment of Plants Along a Fluctuating Water-Depth Gradient, 82, 2216–2232, https://doi.org/10.1890/0012-9658(2001)082[2216:COTEOP]2.0.CO;2, 2001.

Sorrell, B. K., Mendelssohn, I. A., McKee, K. L., and Woods, R. A.: Ecophysiology of Wetland Plant Roots: A Modelling Comparison of Aeration in Relation to Species Distribution, Annals of Botany, 86, 675–685, https://doi.org/10.1006/anbo.2000.1173, 2000.

Strand, V. V.: The influence of ventilation systems on water depth penetration of emergent macrophytes, 47, 1097–1105, https://doi.org/10.1046/j.1365-2427.2002.00834.x, 2002.

Sturtevant, C. S., Oechel, W. C., Zona, D., and Emerson, C. E.: Soil moisture control over autumn season methane flux, Arctic Coastal Plain of Alaska, 8, 6519–6554, https://doi.org/10.5194/bgd-8-6519-2011, 2011.

Sutton-Grier, A. E. and Megonigal, J. P.: Plant species traits regulate methane production in freshwater wetland soils, Soil Biology and Biochemistry, 43, 413–420, https://doi.org/10.1016/j.soilbio.2010.11.009, 2011.

Turetsky, M. R., Kotowska, A., Bubier, J., Dise, N. B., Crill, P., Hornibrook, E. R. C., Minkkinen, K., Moore, T. R., Myers-Smith, I. H., Nykänen, H., Olefeldt, D., Rinne, J., Saarnio, S., Shurpali, N., Tuittila, E.-S., Waddington, J. M., White, J. R., Wickland, K. P., and Wilmking, M.: A synthesis of methane emissions from 71 northern, temperate, and subtropical wetlands, 20, 2183–2197, https://doi.org/10.1111/gcb.12580, 2014.

Valk, A. G. van der, Squires, L., and Welling, C. H.: Assessing the Impacts of an Increase in Water Level on Wetland Vegetation, 4, 525–534, https://doi.org/10.2307/1941954, 1994.

Van Huissteden, K., Hendriks, D., Petrescu, A. M. R., Rebel, K., and Berrittella, C.: Sensitivity analysis of a wetland methane emission process model based on temperate and arctic wetland sites, 2008.

Villa, J., Ju, Y., Rey-Sanchez, A. C., and Bohrer, G.: Plant-mediated methane transport in emergent and floating-leaved species of a temperate freshwater mineral-soil wetland, 2020.

Villa, J. A., Ju, Y., Vines, C., Rey-Sanchez, C., Morin, T. H., Wrighton, K. C., and Bohrer, G.: Relationships Between Methane and Carbon Dioxide Fluxes in a Temperate Cattail-Dominated Freshwater Wetland, 124, 2076–2089, https://doi.org/10.1029/2019JG005167, 2019.

Webb, E. K., Pearman, G. I., and Leuning, R.: Correction of flux measurements for density effects due to heat and water vapour transfer, 106, 85–100, https://doi.org/10.1002/qj.49710644707, 1980.

Zona, D., Oechel, W. C., Kochendorfer, J., U, K. T. P., Salyuk, A. N., Olivas, P. C., Oberbauer, S. F., and Lipson, D. A.: Methane fluxes during the initiation of a large-scale water table manipulation experiment in the Alaskan Arctic tundra, 23, https://doi.org/10.1029/2009GB003487, 2009.

9. Appendices

Appendix A.1 – Parameters

Table A1- 1. Soil related model drivers, by layers. References listed at end of Appendix.

Depth	Bulk Density	Water content at FC	Water content at WP	Vert. sat. hyd. Cond.	Horiz. Sat. hyd. Cond.	Sand content	Silt content	Vol of macropores	Vol of coarse frags	pH	Cat. Exch.
meters	Mg/m^3	m^3/m^3	m^3/m^3	$Mm\ h^{-1}$	$Mm\ h^{-1}$	$g\ kg^{-1}$	$g\ kg^{-1}$	%	%	--	--
Ref.	1	2	2	3	3	3	3	4	4	3	3
0.01	0.75	0.398	0.106	6919.32	6919.3	286.67	210	0	0	7.2	16.5
0.02	0.75	0.398	0.106	6919.32	6919.3	286.67	210	0	0	7.2	16.5
0.04	0.75	0.398	0.106	6851.29	6851.3	281.33	212	0	0	7.15	16.3
0.05	0.75	0.398	0.106	6749.25	6749.3	273.33	215	0	0	7.07	15.9
0.07	0.76	0.398	0.106	6613.2	6613.2	262.67	219	0	0	6.97	15.3
0.1	0.75	0.398	0.106	8925.92	8925.9	201.67	293.33	0	0	6.86	14.8
0.14	0.7	0.398	0.106	10278.01	10278	153.33	354.67	0	0	6.79	13.7
0.2	0.69	0.398	0.106	8662.09	8662.1	220	245	0	0	6.72	11.7
0.29	0.67	0.398	0.106	6986.7	6986.7	173.33	290	0	0	6.8	12.9
0.43	0.57	0.398	0.106	6986.7	6986.7	173.33	290	0	0	6.81	12.9
0.63	0.57	0.398	0.106	6986.7	6986.7	173.33	290	0	0	6.81	12.9
0.93	0.57	0.398	0.106	6986.7	6986.7	173.33	290	0	0	6.81	12.9
1.33	0.57	0.398	0.106	6986.7	6986.7	173.33	290	0	0	6.81	12.9

1.93	0.57	0.398	0.106	6986.7	6986.7	173.33	290	0	0	6.81	12.9
2.83	0.57	0.398	0.106	6986.7	6986.7	173.33	290	0	0	6.81	12.9

Table A1- 2. Soil related model drivers, by layers. References listed at end of Appendix.

Depth	An. Exch.	Aluminum	Iron	Calcium	Magnesium.	Sodium	Potassium	Sulfate	Chloride	Varisciite	Strengite	Moneite
meters	--	gAl/Mg	gFe/Mg	gCa/Mg	gMg/Mg	gNa/Mg	gK/Mg	gS/Mg	gCl/Mg	gP/Mg	gP/Mg	gP/Mg
Ref.	4	3	3	3	3	3	3	3	4	4	4	4
0.01	3	0.7	602.4	0.5	94.5	46.7	66.9	1.8	7.91	50	50	200
0.02	3	0.7	602.4	0.5	94.5	46.7	66.9	1.8	7.91	50	50	200
0.04	3	0.7	604.6	0.5	91.7	44	65.3	1.8	7.91	50	50	200
0.05	3	0.7	607.8	0.4	87.5	39.9	63	1.8	7.91	50	50	200
0.07	3	0.8	612.2	0.4	81.8	34.4	60	1.7	7.9	46.4	46.4	185.7
0.1	3	0.9	623.9	0.4	87	33.8	60	1.6	7.5	25	25	100
0.14	3	1	646.5	0.4	89.6	31.6	57	1.5	7.1	4.2	0	0
0.2	3	1	707.6	0.4	90	25.1	50.8	1.3	7.1	54.3	0	0
0.29	3	1.2	921.3	0.5	103.3	27.7	59.3	1.1	7.1	117.8	0	0
0.43	3	1.2	945	0.5	103.3	27.7	59.3	1	7.1	172.1	0	0
0.63	3	1.2	945	0.5	103.3	27.7	59.3	1	7.1	177.6	0	0
0.93	3	1.2	945	0.5	103.3	27.7	59.3	1	7.1	107	0	0
1.33	3	1.2	945	0.5	103.3	27.7	59.3	1	7.1	90.9	0	0
1.93	3	1.2	945	0.5	103.3	27.7	59.3	1	7.1	109.5	0	0
2.83	3	1.2	945	0.5	103.3	27.7	59.3	1	7.1	121	0	0

Table A1- 3. Soil related model drivers, by layers. References listed at end of Appendix.

Depth	Hydroxyapatite	Al. Hydroxide	Iron Hydrox	Calcite	Gypsum	Gapon activity coeff. Ca--NH_4	Gapon activity coeff. Ca--H	Gapon activity coeff. Ca--Al	Gapon activity coeff. Ca-Mg	Gapon activity coeff. Ca--Na	Gapon activity coeff. Ca--K
meters	gP/Mg	gAl/Mg	gFe/Mg	gCa/Mg	gCa/Mg	--	--	--	--	--	--
Ref.	4	4	4	4	4	4	4	4	4	4	4
0.01	350	1000	2000	0	0	0.01	0.25	0.25	0.6	0.16	3
0.02	350	1000	2000	0	0	0.01	0.25	0.25	0.6	0.16	3
0.04	350	1000	2000	0	0	0.01	0.25	0.25	0.6	0.16	3
0.05	350	1000	2000	0	0	0.01	0.25	0.25	0.6	0.16	3
0.07	325	928.6	1857.1	0	0	0.011	0.25	0.25	0.6	0.16	3
0.1	175	500	1000	0	0	0.0175	0.25	0.25	0.6	0.16	3
0.14	0	0	0	0	0	0.025	0.25	0.25	0.6	0.16	3
0.2	0	0	0	0	0	0.025	0.25	0.25	0.6	0.16	3
0.29	0	0	0	0	0	0.025	0.25	0.25	0.6	0.16	3
0.43	0	0	0	0	0	0.025	0.25	0.25	0.6	0.16	3
0.63	0	0	0	0	0	0.025	0.25	0.25	0.6	0.16	3
0.93	10.4	0	0	0	0	0.025	0.25	0.25	0.6	0.16	3
1.33	40.6	0	0	0	0	0.025	0.25	0.25	0.6	0.16	3
1.93	52.6	0	0	0	0	0.025	0.25	0.25	0.6	0.16	3
2.83	60	0	0	0	0	0.025	0.25	0.25	0.6	0.16	3

Table A1- 4. Typha parameters.

Name	Unit	Value
Rubisco carboxylization activity	µmol g^{-1} s^{-1}	30
Rubisco oxygenation activity	µmol g^{-1} s^{-1}	10
PEP carboxylation activity	µmol g- s^{-1}	0
Km for rubisco carboxylation	µM	12.5
Km for rubisco oxygenation	µM	500
Km for PEP Caroxylation	µM	0
Leaf protein in rubisco	%	12.5
Leaf protein in PEP carboxylase	%	0
Chlorophyll activity	µmol g^{-1} s^{-1}	450
Leaf protein in mesophyll chlorophyll	%	2.5
Leaf protein in bundle sheath chlorophyll	%	0
C_i:C_a ratio	%	70
Primorida initiation rate	$hour^{-1}$	0.015
Leaf appearance rate	$hour^{-1}$	0.009
Chilling temperature	°C	-5
Leafout requirement	hour	120
Leafoff requirement	Hour	240
Leaf length:width ratio	Ratio	15
Branching habit	g g^{-1}	0.33
Plant maturity group	-	Late
Number of primordia in seed	-	2.5
Critical photoperiod	nodes h^{-1}	8
Leaf area:mass	-	0.00417
Petiole length:mass	Ratio	0.5
Leaf area inclined 0°-22.5°	%	0
Leaf area inclined 22.5°-45°	%	0
Leaf area inclined 45°-67.5°	%	50
Leaf area inclined 67.5°-90°	%	50
Clumping factor	-	1
Angle of tillers/branches	°	90
Angles of sheaths/petioles	°	90
Maximum number of fruiting sites per reproductive node	-	3
Maximum number of grain kernel per fruiting site	-	6
Maximum grain kernel mass	gC	0.01
Mass of Carbon storage at planting	gC	1
Maximum rate of kernel filling	gC kernel h^{-1}	0.00002
Initial standing dead biomass	gC m^{-2}	100
Radius of primary roots	m	0.0005
Radius of secondary roots	m	0.0002
Root porosity	m^3 m^{-3}	0.49

Name	Unit	Value
Branching habit	$g\ g^{-1}$	0.05
Root radial resistivity	$Mpa\ h\ m^{-2}$	10000
Root axial resistivity	$Mpa\ h\ m^{-4}$	400000000
Branching frequency primary	m^{-1}	250
Branching frequency secondary	m^{-1}	250
Maximum NH_4-N uptake rate	$g\ m^{-2}\ h^{-1}$	5000
K_m for NH_4-N uptake	$g\ m^{-3}$	0.5
Minimum NH_4-N concentration for uptake	$g\ m^{-3}$	0.0125
Maximum NO_3-N uptake rate	$g\ m^{-2}\ h^{-1}$	0.005
K_m for NO_3-N uptake	$g\ m^{-3}$	0.35
Minimum NO_3-N concentration for uptake	$g\ m^{-3}$	0.03
Maximum PO_4-P uptake rate	$g\ m^{-2}\ h^{-1}$	0.001
K_m for PO_4-P uptake	$g\ m^{-3}$	0.075
Minimum PO_4-P concentration for uptake	$g\ m^{-3}$	0.002
Maximum osmotic potential	Mpa	-1
Shape parameters for stomatal resistance	-	-4
Leaf cuticular resistance	$s\ m^{-1}$	2000

Table A1- 5. Sub-aquatic vegetation parameters.

Name	Unit	Value
Rubisco carboxylization activity	µmol g^{-1} s^{-1}	45
Rubisco oxygenation activity	µmol g^{-1} s^{-1}	9.5
PEP carboxylation activity	µmol g- s^{-1}	0
Km for rubisco carboxylation	µM	12.5
Km for rubisco oxygenation	µM	500
Km for PEP Caroxylation	µM	0
Leaf protein in rubisco	%	12.5
Leaf protein in PEP carboxylase	%	0
Chlorophyll activity	µmol g^{-1} s^{-1}	405
Leaf protein in mesophyll chlorophyll	%	2.5
Leaf protein in bundle sheath chlorophyll	%	0
C_i:C_a ratio	%	70
Primorida initiation rate	$hour^{-1}$	0.015
Leaf appearance rate	$hour^{-1}$	0.009
Chilling temperature	°C	-10
Leafout requirement	hour	24
Leafoff requirement	Hour	840
Leaf length:width ratio	Ratio	1
Branching habit	g g^{-1}	1
Plant maturity group	-	Early
Number of primordia in seed	-	2.5
Critical photoperiod	nodes h^{-1}	Summer solstice
Leaf area:mass	-	0.00167
Petiole length:mass	Ratio	0.0125
Leaf area inclined 0°-22.5°	%	0.25
Leaf area inclined 22.5°-45°	%	0.25
Leaf area inclined 45°-67.5°	%	0.25
Leaf area inclined 67.5°-90°	%	0.25
Clumping factor	-	1
Angle of tillers/branches	°	90
Angles of sheaths/petioles	°	0
Maximum number of fruiting sites per reproductive node	-	10
Maximum number of grain kernel per fruiting site	-	10
Maximum grain kernel mass	gC	0.001
Mass of Carbon storage at planting	gC	0.001
Maximum rate of kernel filling	gC kernel h^{-1}	0.0000025

Name	Unit	Value
Initial standing dead biomass	gC m^{-2}	0
Radius of primary roots	m	0.0001
Radius of secondary roots	m	0.00005
Root porosity	m^3 m^{-3}	0
Branching habit	g g^{-1}	0.1
Root radial resistivity	Mpa h m^{-2}	10000
Root axial resistivity	Mpa h m^{-4}	4000000000
Branching frequency primary	m^{-1}	250
Branching frequency secondary	m^{-1}	250
Maximum NH_4-N uptake rate	g m^{-2} h^{-1}	0
K_m for NH_4-N uptake	g m^{-3}	0.4
Minimum NH_4-N concentration for uptake	g m^{-3}	0.0125
Maximum NO_3-N uptake rate	g m^{-2} h^{-1}	0
K_m for NO_3-N uptake	g m^{-3}	0.35
Minimum NO_3-N concentration for uptake	g m^{-3}	0.03
Maximum PO_4-P uptake rate	g m^{-2} h^{-1}	0.001
K_m for PO_4-P uptake	g m^{-3}	0.075
Minimum PO_4-P concentration for uptake	g m^{-3}	0.002
Maximum osmotic potential	Mpa	-1.25
Shape parameters for stomatal resistance	-	0
Leaf cuticular resistance	s m^{-1}	500

Table A1- 6. Broadleaf tree parameters.

Name	Unit	Value
Rubisco carboxylization activity	µmol g^{-1} s^{-1}	45.0
Rubisco oxygenation activity	µmol g^{-1} s^{-1}	9.5
PEP carboxylation activity	µmol g- s^{-1}	0
Km for rubisco carboxylation	µM	12.5
Km for rubisco oxygenation	µM	500
Km for PEP Caroxylation	µM	0
Leaf protein in rubisco	%	0.125
Leaf protein in PEP carboxylase	%	0
Chlorophyll activity	µmol g^{-1} s^{-1}	405
Leaf protein in mesophyll chlorophyll	%	0.025
Leaf protein in bundle sheath chlorophyll	%	0
C_i:C_a ratio	%	0.7
Primorida initiation rate	$hour^{-1}$	0.015
Leaf appearance rate	$hour^{-1}$	0.009
Chilling temperature	°C	-5.0
Leafout requirement	hour	240
Leafoff requirement	Hour	240
Leaf length:width ratio	Ratio	4
Branching habit	g g^{-1}	1
Plant maturity group	-	8
Number of primordia in seed	-	2.5
Critical photoperiod	nodes h^{-1}	-1.0
Leaf area:mass	-	0.009
Petiole length:mass	Ratio	0.015
Leaf area inclined 0°-22.5°	%	0.25
Leaf area inclined 22.5°-45°	%	0.25
Leaf area inclined 45°-67.5°	%	0.25
Leaf area inclined 67.5°-90°	%	0.25
Clumping factor	-	0.65
Angle of tillers/branches	°	90
Angles of sheaths/petioles	°	0
Maximum number of fruiting sites per reproductive node	-	0.5
Maximum number of grain kernel per fruiting site	-	1
Maximum grain kernel mass	gC	0.10
Mass of Carbon storage at planting	gC	10.0
Maximum rate of kernel filling	gC kernel h^{-1}	0.0002
Initial standing dead biomass	gC m^{-2}	5000
Radius of primary roots	m	0.0010
Radius of secondary roots	m	0.0002
Root porosity	m^3 m^{-3}	0

Name	Unit	Value
Branching habit	$g\ g^{-1}$	0.1
Root radial resistivity	$Mpa\ h\ m^{-2}$	10000
Root axial resistivity	$Mpa\ h\ m^{-4}$	4×10^{9}
Branching frequency primary	m^{-1}	250
Branching frequency secondary	m^{-1}	250
Maximum NH_4-N uptake rate	$g\ m^{-2}\ h^{-1}$	0.005
K_m for NH_4-N uptake	$g\ m^{-3}$	0.4
Minimum NH_4-N concentration for uptake	$g\ m^{-3}$	0.0125
Maximum NO_3-N uptake rate	$g\ m^{-2}\ h^{-1}$	0.005
K_m for NO_3-N uptake	$g\ m^{-3}$	0.35
Minimum NO_3-N concentration for uptake	$g\ m^{-3}$	0.03
Maximum PO_4-P uptake rate	$g\ m^{-2}\ h^{-1}$	0.001
K_m for PO_4-P uptake	$g\ m^{-3}$	0.075
Minimum PO_4-P concentration for uptake	$g\ m^{-3}$	0.002
Maximum osmotic potential	Mpa	-1.25
Shape parameters for stomatal resistance	-	-5.0
Leaf cuticular resistance	$s\ m^{-1}$	2000

Table A1- 7. Typha organ characteristics parameters.

	Unit	Leaf	Sheath / petiole	Stalk	Reserve	Husk / pod	Ear	Grain	Root	Nodule
Growth yield	$gC\ gC^{-1}$	0.72	0.76	0.8	0.88	0.76	0.76	0.88	0.76	0.72
N:C ratio	$gN\ gC^{-1}$	0.1	0.02	0.01	0.025	0.02	0.02	0.033	0.02	0.1
P:C ratio	$gP\ gC^{-1}$	0.01	0.002	0.001	0.0025	0.002	0.002	0.0033	0.002	0.01

*Reference key for Appendix tables
1 – (Bernal and Mitsch, 2008)
2 – SPAW model (Saxton and Rawls, 2006)
3 –Soil cores drawn for this study
4 – (Mekonnen et al., 2016)
5 – Assumed based on site conditions

Appendix A.2 – Climate forcing

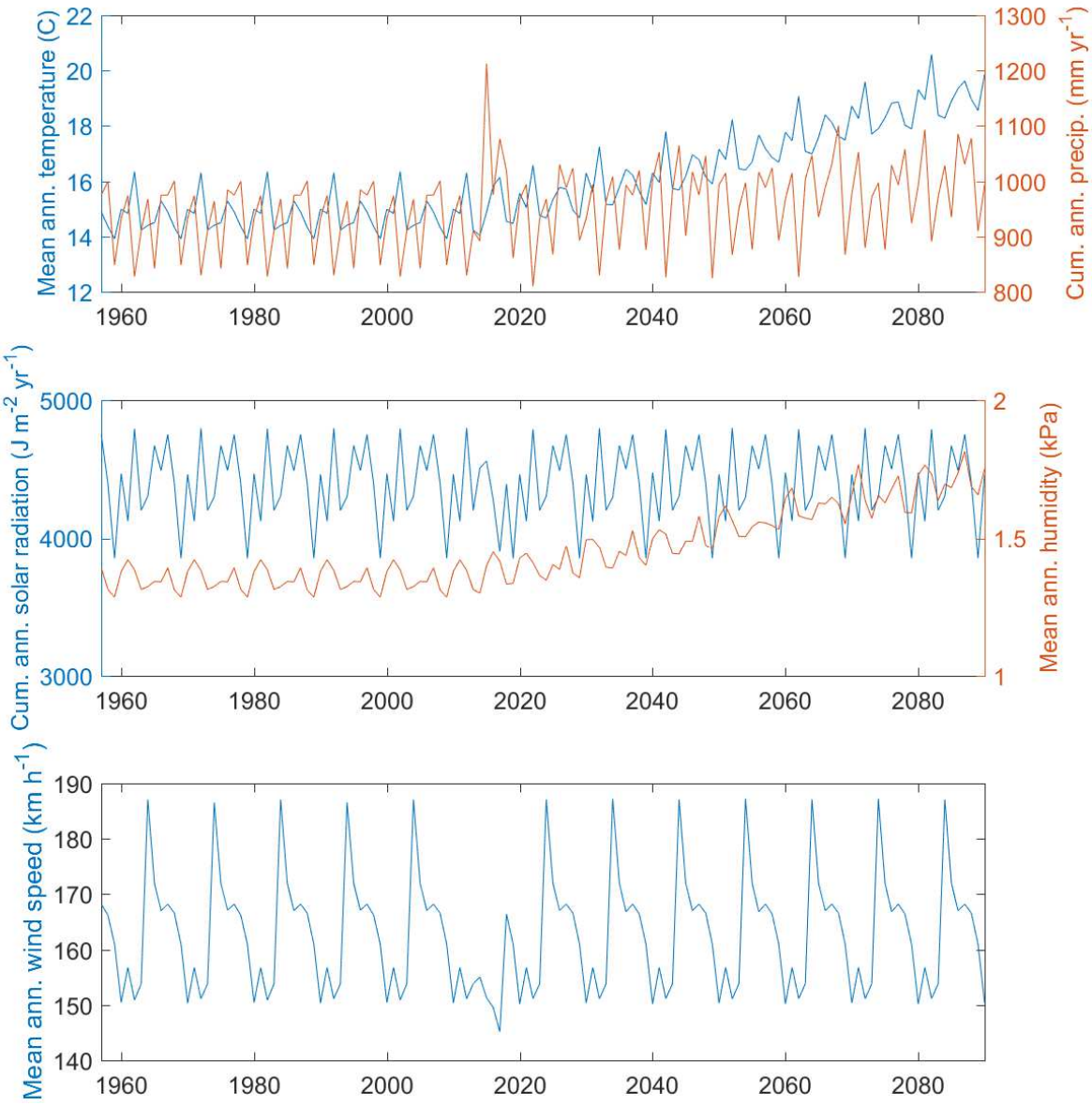

Figure A2- 1. Meteorological data used to drive ecosys through the full simulation.

Appendix A.3 – Empirical model selection

Wetland water depth model

Our empirical model for wetland water depth indicated that the interaction of Lake Erie's water depth with the cumulative time since a breach or fill event (t_{breach}) gave the highest explanatory power to the empirical model, consistent with the hydrological link when the sand barrier is breached. The second most effective variable was the Lake Erie water depth, which likely resulted from groundwater linkages that affected OWC water depths at all times. Air temperature had the third highest explanatory power, likely as a proxy for seasonality, and the fourth highest explanatory power was from cumulative precipitation since the breach. Interestingly, instantaneous precipitation did not have a significant effect, as indicated by an increase in the AIC value when this variable is included. We hypothesize that the predictive power that precipitation would have given is conflated with the time since breach, since precipitation can affect whether the sand barrier breaches or reforms. Humidity and PAR were considered as proxy variables for transpiration, but neither increased the model's forecasting ability, and thus were rejected by our selection criteria.

Table A3.1. Goodness of fit for a stepwise linear model for predicting OWC water depth organized by explanatory power using half-hourly predictor variables. Here Erie Level means Lake Erie water depth, t_{breach} is the time since the last breach formation or fill, Temperature is the water temperature at 10 cm, Rain accumulation is the accumulated precipitation since the last breach formation or fill, RH is the relative humidity, and PAR is the photosynthetically available radiation. Bold red values were rejected as they failed the AIC metric of the whole model.

Number of variables	Variable added	r^2	AIC
1	Erie Level × t_{breach}	0.11	-723.91
2	Erie Level	0.28	-1330.71
3	t_{breach}	0.32	-1494.90
4	Water temperature	0.35	-1551.90
5	Rain accumulation since t_{breach}	0.36	-1557.28
6	Precipitation rate	0.36	**-1554.16**
6	RH	0.36	**-1556.68**
6	PAR	0.36	**-1415.74**

Wetland vegetation cover empirical model

Our empirical model for wetland vegetation only selected water depth as a predictor variable. Including either DO or temperature as a predictor variable would have improved r^2 (to 0.69 or 0.50, respectively), but in both cases the AIC indicated that the inclusion of the new variable into the empirical model was not justified, and therefore, we excluded both from the final model (Table 2). Our finding that water depth controls plant community structure is consistent with other studies (Casanova and Brock,

2000; Poiani and Johnson, 1993). Although water depth itself is only an indirect controlling variable, it has been shown to affect reemergence and shoot density of emergent plants (Valk et al., 1994). Increased water depth increases light extinction through the water column, resulting in less incoming solar radiation to the soil, and provides a thermal barrier, both of which may inhibit plant growth. Therefore, water depth is an indirect proxy for several variables that may influence wetland plant-community composition.

Table A3.2. Empirical model for plant community structure of the wetland. Bold red values were not accepted into the final model since the AIC score increased as those variables were added, indicating that the additional explanatory power of those variables was outweighed by the cost of including another variable in the empirical model.

Number of variables	Variable name	r^2	AIC
1	Depth	0.49	-10.70
2	Temperature	0.50	**-8.74**
2	Dissolved Oxygen	0.69	**-9.51**

Appendix A.4 – Model validation

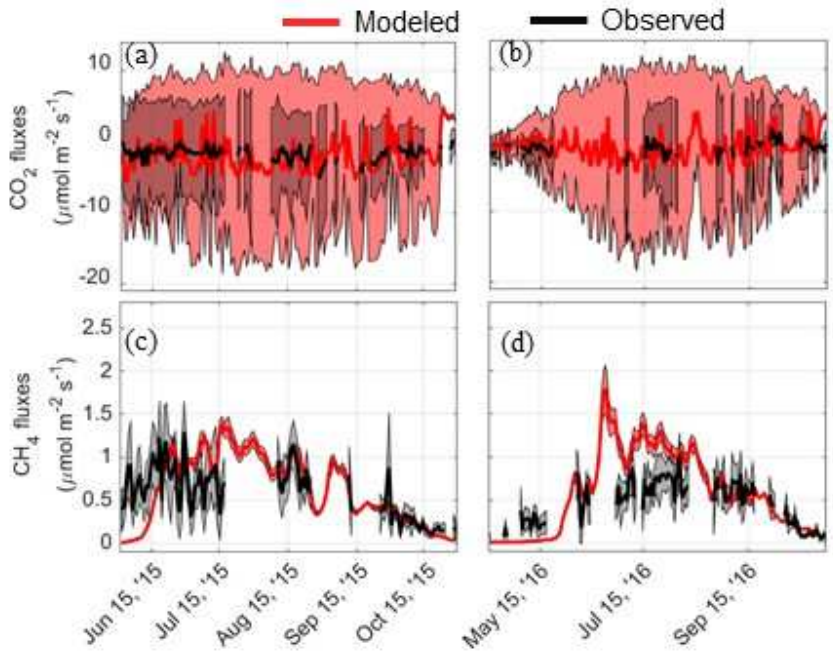

Figure A4.1 - Growing season modeled (red) and observed (black) daily average (a) CO_2 fluxes for 2015 and (b) 2016 and CH_4 fluxes during (c) 2015 and (d) 2016 growing seasons. Shaded areas show the standard deviation of hourly fluxes within each day. Modeled CO_2 fluxes closely match observations while the model overestimated observed methane fluxes, but reproduced the seasonal trend.

Comparisons of modeled and observed fluxes at daily time scales are useful to determine the seasonal fit of data, particularly when hourly data are highly variable, as is the case with CH_4 flux observations here. When comparing *ecosys* to daily fluxes, we filtered to only days with greater than 50% of data available and gap-filled through the nighttime periods using a neural network to avoid biasing towards high daytime measurements. Eddy covariance gap-filling methodologies have far higher uncertainties associated with them than observations, and so comparing to the daily flux measurements should be done in conjunction with examining hourly measurements (e.g. Figure 5).

After adjusting the modeled fluxes for the footprint mixing of disparate terrain types observed at the eddy covariance tower, modeled CH_4 fluxes generally agreed with observations, though biased upwards (Figure A4.1 panels c and d). Although both modeled CO_2 and CH_4 fluxes had bias from the observations, the biases were in opposite direction and changing uncertain model drivers to adjust for one bias necessarily meant increasing the bias in the other. Adjusting model files by altering the soil carbon to nitrogen ratio, for example, would create larger CO_2 fluxes resulting in increased organic carbon availability for methanogens and therefore larger methane fluxes. Similarly, reducing CH_4 fluxes closer to reality effectively forced us to further underestimate the footprint weighted mixture of CO_2 fluxes. Because of this, we adjusted model drivers such as soil C:N ratio such that we would strike a balance

between CO_2 fluxes and CH_4 flux accuracy. Beyond these biases, our observed CH_4 fluxes also showed far more variability than CO_2 fluxes, with large standard deviations at short (e.g., hourly) time spans.

We also validated our model by comparing our thermodynamic simulations of soil temperatures to those observed in the vicinity of the eddy covariance tower (Figure A4.2). Measured and modeled soil temperatures matched well, especially for 2016. Simulated soil temperatures varied slightly depending on the vegetation cover of the model patch.

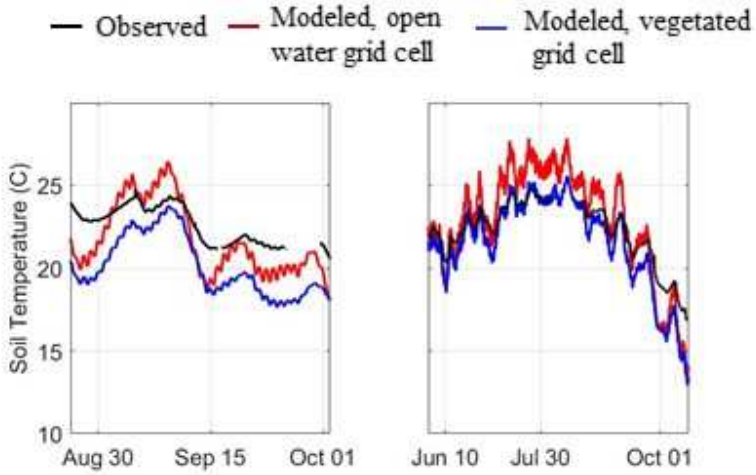

Figure A4.2. Modeled (blue for vegetated grid cell, red for open water grid cell) and observed (black) 10 cm depth soil temperature. Since there was no soil layer centered on 10 cm, we interpolated the modeled temperature from neighboring soil layers. Fit showed high agreement, suggesting thermodynamics of the model are well represented at the site.

How do wetland water depths affect wetland surface CO_2 and CH_4 fluxes?

Methods

NOAA projections of Lake Erie Water Level

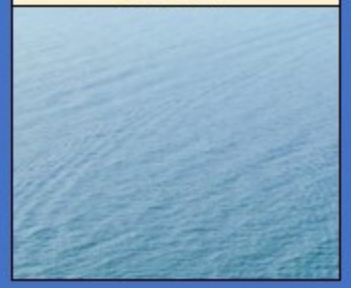

Aerial observations of vegetation cover

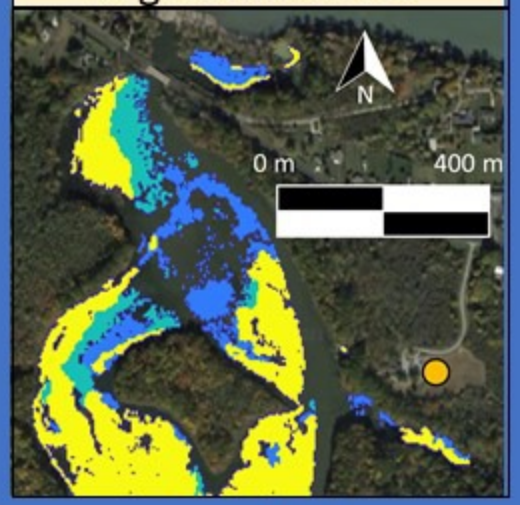

Eddy covariance measurements of CH_4 and CO_2 fluxes

Mechanistic model, *ecosys*

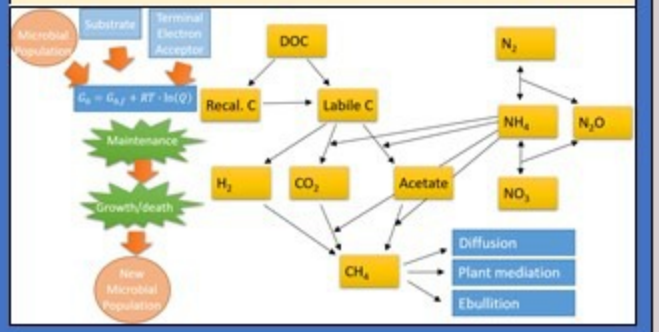

Findings

- Water level of Lake Erie directly affects water level of wetland
- Wetland water depth affects where plants can and cannot grow
- Wetland CO_2 and CH_4 fluxes likely to increase in magnitude with increasing temperatures
- In scenarios where wetland dries out, we expect large decreases in wetland CH_4 simultaneous with large effluxes of CO_2 associated with oxidizing stored carbon